© 2014. Published by The Company of Biologists Ltd | Development (2014) 141, 795-806 doi:10.1242/dev.101907

RESEARCH ARTICLE

STEM CELLS AND REGENERATION

Integrin $\alpha_v\beta_3$ and thyroid hormones promote expansion of progenitors in embryonic neocortex

Denise Stenzel[1], Michaela Wilsch-Bräuninger[1], Fong Kuan Wong[1], Heike Heuer[2] and Wieland B. Huttner[1,*]

ABSTRACT

Neocortex expansion during evolution is associated with the enlargement of the embryonic subventricular zone, which reflects an increased self-renewal and proliferation of basal progenitors. In contrast to human, the vast majority of mouse basal progenitors lack self-renewal capacity, possibly due to lack of a basal process contacting the basal lamina and downregulation of cell-autonomous production of extracellular matrix (ECM) constituents. Here we show that targeted activation of the ECM receptor integrin $\alpha_v\beta_3$ on basal progenitors in embryonic mouse neocortex promotes their expansion. Specifically, integrin $\alpha_v\beta_3$ activation causes an increased cell cycle re-entry of Pax6-negative, Tbr2-positive intermediate progenitors, rather than basal radial glia, and a decrease in the proportion of intermediate progenitors committed to neurogenic division. Interestingly, integrin $\alpha_v\beta_3$ is the only known cell surface receptor for thyroid hormones. Remarkably, tetrac, a thyroid hormone analog that inhibits the binding of thyroid hormones to integrin $\alpha_v\beta_3$, completely abolishes the intermediate progenitor expansion observed upon targeted integrin $\alpha_v\beta_3$ activation, indicating that this expansion requires the binding of thyroid hormones to integrin $\alpha_v\beta_3$. Convergence of ECM and thyroid hormones on integrin $\alpha_v\beta_3$ thus appears to be crucial for cortical progenitor proliferation and self-renewal, and hence for normal brain development and the evolutionary expansion of the neocortex.

KEY WORDS: Cortical neurogenesis, Integrins, Thyroid hormones, Mouse

INTRODUCTION

The profound increase in relative brain size during evolution, notably the expansion of the neocortex, underlies the increased cognitive abilities in humans. This expansion is thought to be primarily due to an increase in the proliferation and self-renewal capacity of neural stem and progenitor cells (NSPCs) during fetal development (Kriegstein et al., 2006; Fish et al., 2008; Rakic, 2009; Fietz and Huttner, 2011; Lui et al., 2011; Borrell and Reillo, 2012; Franco and Müller, 2013). [Throughout this study, the term 'proliferation' is not used for any mode of cell division, but only for that through which the number of a given NSPCs type is increased (i.e. symmetric proliferative division); likewise, the term 'self-renewal' is only used for that mode of cell division through which the number of a given NSPCs type remains constant, but is not increased (i.e. asymmetric self-renewing division).]

There are two principal classes of NSPCs that generate the projection neurons of the neocortex, referred to as apical and basal progenitors. Apical progenitors (APs) undergo mitosis at the ventricular (apical) surface of the cortical wall (Fietz and Huttner, 2011). APs comprise, in particular, apical radial glial cells (aRGCs), the nuclei of which reside in the ventricular zone (VZ) (Götz and Huttner, 2005; Kriegstein and Alvarez-Buylla, 2009; Shitamukai and Matsuzaki, 2012).

Basal progenitors (BPs) originate from APs, delaminate from the ventricular surface, and undergo mitosis at an abventricular location, typically in the subventricular zone (SVZ), a second germinal layer located basally to the VZ (Götz and Huttner, 2005; Pontious et al., 2008; Kriegstein and Alvarez-Buylla, 2009; Fietz and Huttner, 2011; Borrell and Reillo, 2012). There are three main types of BP: (1) basal (or outer) radial glial cells (bRGCs); (2) transit-amplifying progenitors (TAPs); and (3) intermediate progenitor cells (IPCs). bRGCs are polarized, process-bearing cells (Fietz et al., 2010; Hansen et al., 2010; Reillo et al., 2011; Betizeau et al., 2013), whereas both TAPs and IPCs lack apical and basal processes and the corresponding cell polarity at mitosis (Haubensak et al., 2004; Noctor et al., 2004; Attardo et al., 2008). bRGCs and TAPs undergo more than one round of cell division, whereas IPCs typically divide only once, generating two postmitotic neurons (Haubensak et al., 2004; Miyata et al., 2004; Noctor et al., 2004; Hansen et al., 2010; Shitamukai et al., 2011; Wang et al., 2011; Betizeau et al., 2013).

Both mouse and human aRGCs are endowed with proliferation and self-renewal capacity. By contrast, there is a profound difference regarding this capacity between mouse and human BPs. The vast majority of mouse BPs are IPCs, with bRGCs and TAP-like cells constituting only minor proportions (Haubensak et al., 2004; Miyata et al., 2004; Noctor et al., 2004; Attardo et al., 2008; Shitamukai et al., 2011; Wang et al., 2011; Kelava et al., 2012), and thus most mouse BPs lack proliferation and self-renewal capacity. By contrast, most human BPs are bRGCs and TAPs (Fietz et al., 2010; Hansen et al., 2010) and thus exhibit proliferation and self-renewal capacity. Similar observations have recently been reported for the macaque monkey (Betizeau et al., 2013). Indeed, an increased proliferation and self-renewal capacity of BPs, resulting in enlargement of the embryonic SVZ, is thought to be a main cause of neocortex expansion during evolution (Fietz and Huttner, 2011; Lui et al., 2011; Borrell and Reillo, 2012). The proliferation and self-renewal capacity of bRGCs is thought to be due, at least in part, to these cells extending processes, specifically a basal process towards the basal lamina (Fietz et al., 2010; Hansen et al., 2010; Reillo et al., 2011; Shitamukai et al., 2011; Wang et al., 2011; Kelava et al., 2012; Betizeau et al., 2013). This may allow bRGCs to receive proliferative signals from extracellular matrix (ECM) constituents of the basal lamina (Fietz et al., 2010). This notion extends a concept based on findings with mouse aRGCs, which have implicated the basal process in their self-renewal (Konno et al., 2008; Kosodo and Huttner, 2009; Loulier et al., 2009; Shitamukai et al., 2011) and which have shown that basal lamina contact, laminin α_2 and α_4, and integrin β_1 are crucial for aRGC survival (Radakovits et al., 2009).

[1]Max Planck Institute of Molecular Cell Biology and Genetics, Pfotenhauerstrasse 108, 01307 Dresden, Germany. [2]Leibniz Institute for Age Research / Fritz Lipmann Institute (FLI), Beutenbergstrasse 11, 07745 Jena, Germany.

*Author for correspondence (huttner@mpi-cbg.de)

Received 29 July 2013; Accepted 28 November 2013

Development (2014) doi:10.1242/dev.101907

However, it is unknown why BPs that lack basal lamina contact have greater proliferative potential in human (or macaque) than in mouse. Recently, our group reported on the transcriptomes of the VZ versus SVZ in mouse versus human developing neocortex (Fietz et al., 2012), as well as on the transcriptomes of mouse cortical progenitors undergoing proliferative versus neurogenic divisions (Arai et al., 2011). The data obtained suggest that the greater proliferation and self-renewal capacity of human than mouse BPs, and of mouse aRGCs than IPCs, may be linked to progenitor-autonomous ECM production (Arai et al., 2011; Fietz et al., 2012). These findings prompted us to investigate whether the targeted activation of ECM receptors, notably integrin $\alpha_v\beta_3$ (itgαvβ3) (for the reasons outlined below), in the developing mouse neocortex can induce BP proliferation.

RESULTS

Expression of itgαvβ3 in mouse VZ and SVZ, and APs and BPs

In light of the potential importance of ECM constituents for BP proliferation and self-renewal capacity, we focused on integrins, a family of heterodimers comprised of an alpha (α) and a beta (β) subunit that constitute the main cell surface receptors for ECM constituents. Previous studies have concentrated on α_6- and β_1-containing integrins and demonstrated an involvement of the β_1 subunit in aRGC proliferation and survival (Haubst et al., 2006; Lathia et al., 2007; Loulier et al., 2009; Radakovits et al., 2009). In the present study, we chose to investigate itgαvβ3, for two reasons. First, the SVZ of developing ferret neocortex, in contrast to embryonic mouse neocortex, contains a high relative abundance of bRGCs (Fietz et al., 2010; Reillo et al., 2011). Remarkably, interference with itgαvβ3 that is expressed on ferret bRGCs inhibits their proliferation and self-renewal capacity (Fietz et al., 2010).

Second, previous transcriptome analyses (Arai et al., 2011; Fietz et al., 2012) show that there is lower, albeit still detectable, expression of itgαv and itgβ3 in neurogenic compared with proliferating progenitors in mouse (Arai et al., 2011) (supplementary material Fig. S1A), and of itgαv in the mouse SVZ compared with VZ (Fietz et al., 2012) (supplementary material Fig. S1B), whereas itgαv expression is maintained in the human OSVZ compared to VZ (Fietz et al., 2012) (supplementary material Fig. S1B). Complementing and extending these transcriptome data, conventional immunofluorescence (supplementary material Fig. S1A-G) and correlative immunofluorescence and immunogold electron microscopy (supplementary material Fig. S1H-L) for itgβ3 revealed its presence in embryonic day (E)14.5 mouse neocortex. Taken together, these results show that compared with aRGCs, mouse BPs contain lower, but detectable, levels of itgαv and itgβ3. Hence, given that itgαv is a major heterodimerizing subunit for itgβ3 (Hynes, 2002), itgαvβ3 emerges as a prime candidate to promote mouse BP proliferation when activated.

Targeted activation of itgαvβ3 increases mitotic APs and BPs

To activate itgαvβ3, we used the activating antibody LIBS-6 (Frelinger et al., 1991; Tzima et al., 2001). Using this 'pharmacological' approach, we are able to acutely manipulate itgαvβ3 activation at any desired developmental stage. Further, the LIBS-6 antibody represents a highly specific tool, similar to a dominant-active itgαvβ3. However, delivering expression constructs for itgαvβ3 or a dominant-active form of it to the mouse embryonic neocortex (e.g. by electroporation) would primarily target aRGCs and would affect BPs only as a consequence. In contrast, administration of the LIBS-6 antibody allows the activation of itgαvβ3 directly on BPs, as antibodies are known to diffuse across developing neocortical tissue (Loulier et al., 2009).

Integrin activation was examined using hemisphere rotation (HERO) culture of E14.5 mouse cerebral cortex, which faithfully reproduces *in utero* cortical development with regard to neural progenitor proliferation and differentiation (Schenk et al., 2009). We first verified that integrins, in general (and not necessarily on progenitors only), could be activated under our experimental conditions, using an established treatment, addition of manganese (Mn^{2+}) (Cluzel et al., 2005; Afshari et al., 2010), and quantifying phosphoERK levels (supplementary material Fig. S2A,B). Next, we found that LIBS-6 treatment increased phosphoERK levels to an extent consistent with the relative abundance of *itgαv* mRNA present in the E14.5 mouse neocortex (supplementary material Fig. S2C,D), suggesting that LIBS-6 treatment can be used to activate itgαvβ3.

Activation of itgαvβ3 by LIBS-6 increased the level of mitotic APs and, even more so, of mitotic BPs (Fig. 1A-C) (for definition of progenitor types, see Material and Methods). Specifically, immunofluorescence for phosphohistone H3 (Fig. 1A) and phosphovimentin (see Fig. 3D,E), markers of mitotic cells, revealed that LIBS-6 treatment in HERO culture for 24 hours (Fig. 1B,C) and 48 hours (see Fig. 3B,C,E), respectively, increased the number of mitoses observed at the ventricular surface by one-third (Fig. 1B) and almost doubled those in the SVZ and basal VZ (Fig. 1C, Fig. 3B).

These effects of itgαvβ3 activation on AP and BP proliferation were accompanied by changes in the radial versus lateral extension of the developing cortical wall. Compared with HERO culture for 24 hours in the presence of mouse isotype control IgG (ctrl IgG), the cortical wall upon LIBS-6 treatment was reduced in thickness (Fig. 1D,E) and increased in lateral length (Fig. 1D,F). The reduction in the radial dimension (Fig. 1D,E) largely reflected a compaction of the VZ, which showed a significant decrease in thickness (Fig. 1G,H), but without a decrease in the number of nuclei per radial field (Fig. 1G,I). Given the increase in the lateral length of the cortical wall upon LIBS-6 treatment (Fig. 1D,F), the constant density of nuclei per radial field in the VZ, SVZ+IZ and cortical plate (CP) implies that the population size of all, APs, BPs and neurons, was increased by itgαvβ3 activation. This increase in population size should be borne in mind with regard to all effects of itgαvβ3 activation described below, as the various parameters studied are quantified per microscopic or radial field, and hence the total magnitude of a given increase is greater, and that of a given decrease smaller, than depicted by such quantification.

Itgαvβ3 activation increases BP proliferation

To further investigate the effect of itgαvβ3 activation on AP and BP proliferation, we applied the thymidine analog 5-ethynyl-2′-deoxyuridine (EdU) for 1 hour before the end of a 48-hour HERO culture to determine the number of cortical progenitors in S-phase. Itgαvβ3 activation by LIBS-6 resulted in an increased number of EdU-positive (EdU+) progenitors in the VZ and SVZ compared with ctrl IgG (Fig. 2A,B). No significant difference in apoptosis between control and LIBS-6–treated hemispheres was observed (supplementary material Fig. S3), and so altered apoptosis could not account for the increase in EdU+ cells.

To gain insight into which types of progenitors were affected by itgαvβ3 activation, we analyzed EdU+ nuclei for the presence or absence of the marker Pax6 (Englund et al., 2005; Osumi et al., 2008) (Fig. 2C,D,F). Strongly Pax6-positive (Pax6+) nuclei in the VZ (Fig. 2F) were considered to belong to aRGCs. Pax6+ nuclei in the SVZ, the immunoreactivity signal of which was generally lower

Development (2014) doi:10.1242/dev.101907

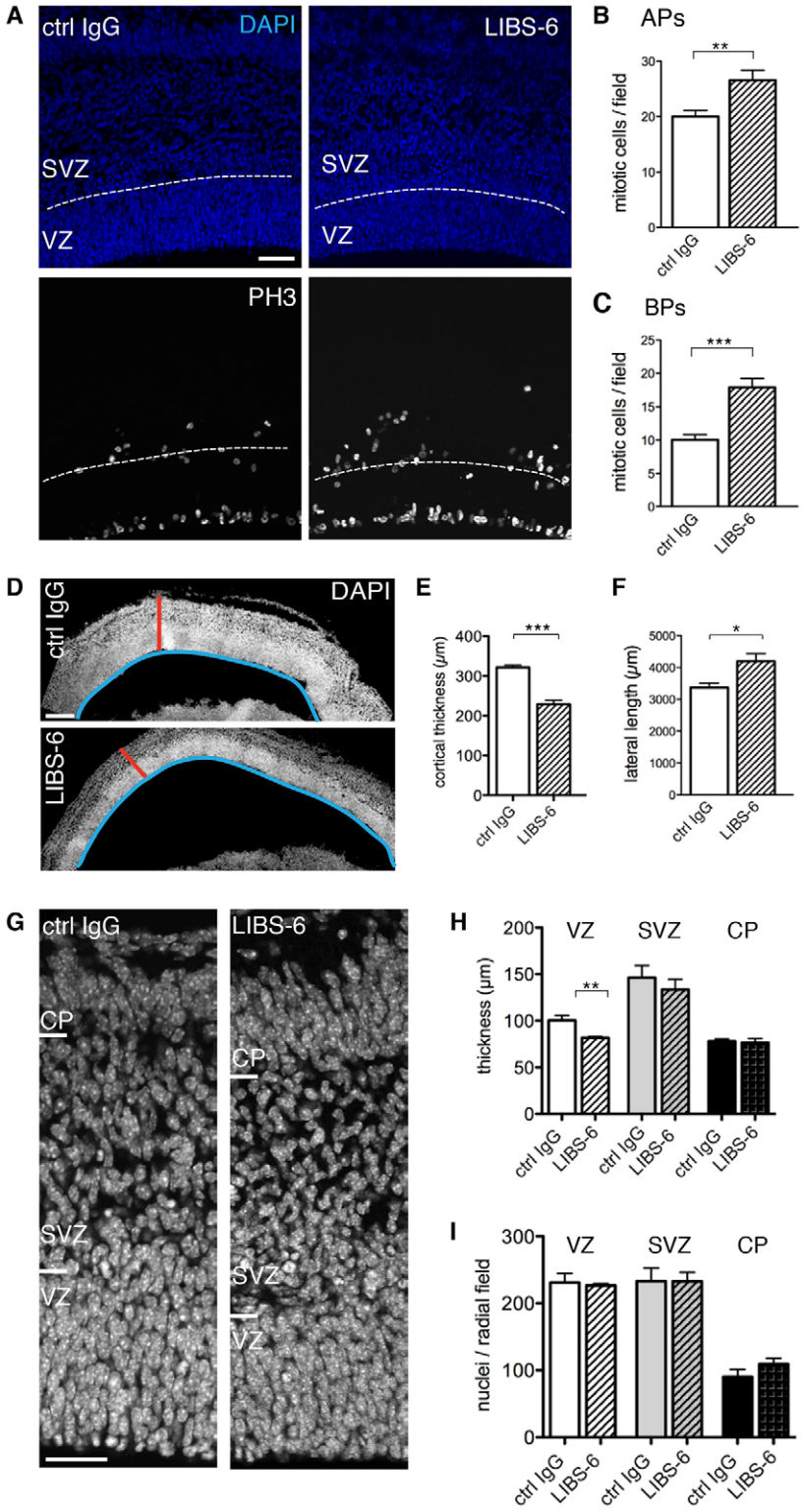

Fig. 1. Itgαvβ3 activation increases cortical progenitor proliferation. (A-I) 24-hour HERO culture of E14.5 mouse dorsal telencephalon with control (ctrl) IgG or LIBS-6. (A) Phosphohistone H3 (PH3) immunofluorescence (white) and 4′,6-diamidino-2-phenylindole (DAPI) staining (blue) (single 1.91-μm optical sections); dashed lines, boundary of VZ and SVZ. (B,C) Mitotic APs (B) and BPs (C) per field (360×360 μm); mean of six hemispheres. (D) DAPI-stained neocortex (sagittal sections, 4-μm stacks). Red bars, cortical thickness; blue lines, lateral length. (E,F) Cortical thickness (E) and cortical lateral length (F). Mean of three to five hemispheres. (G) DAPI-stained neocortex (single 1-μm optical sections). (H) Radial thickness of cortical zones. 'SVZ' includes intermediate zone. Mean of three to five hemispheres. (I) Nuclei per radial field in each cortical zone; mean of six hemispheres. Scale bars: 50 μm in A; 200 μm in D; 35 μm in G.

than that of the VZ nuclei (Fig. 2D), were considered to belong to either bRGCs (Shitamukai et al., 2011; Wang et al., 2011) or IPCs that had inherited some Pax6 protein from aRGCs (Fish et al., 2008; Arai et al., 2011). Pax6-negative (Pax6–) nuclei in the VZ and SVZ were considered to belong to newborn and fully delaminated, respectively, IPCs and TAPs (Englund et al., 2005). LIBS-6 treatment caused an almost twofold increase in the weakly Pax6+ & EdU+ nuclei in the SVZ (Fig. 2E, left) and a profound, fivefold increase in the Pax6– EdU+ nuclei in that germinal zone (Fig. 2E, right). Although not statistically significant, a trend towards the latter BP increase could already by observed in the VZ (Fig. 2G, right). Pax6+ EdU+ nuclei in the VZ, i.e. aRGCs, appeared to show a moderate (not statistically significant) increase upon LIBS-6 treatment (Fig. 2G, left).

We noticed that the fold-increase in Pax6– EdU+ progenitors in the SVZ upon itgαvβ3 activation, which accounted for

Development (2014) doi:10.1242/dev.101907

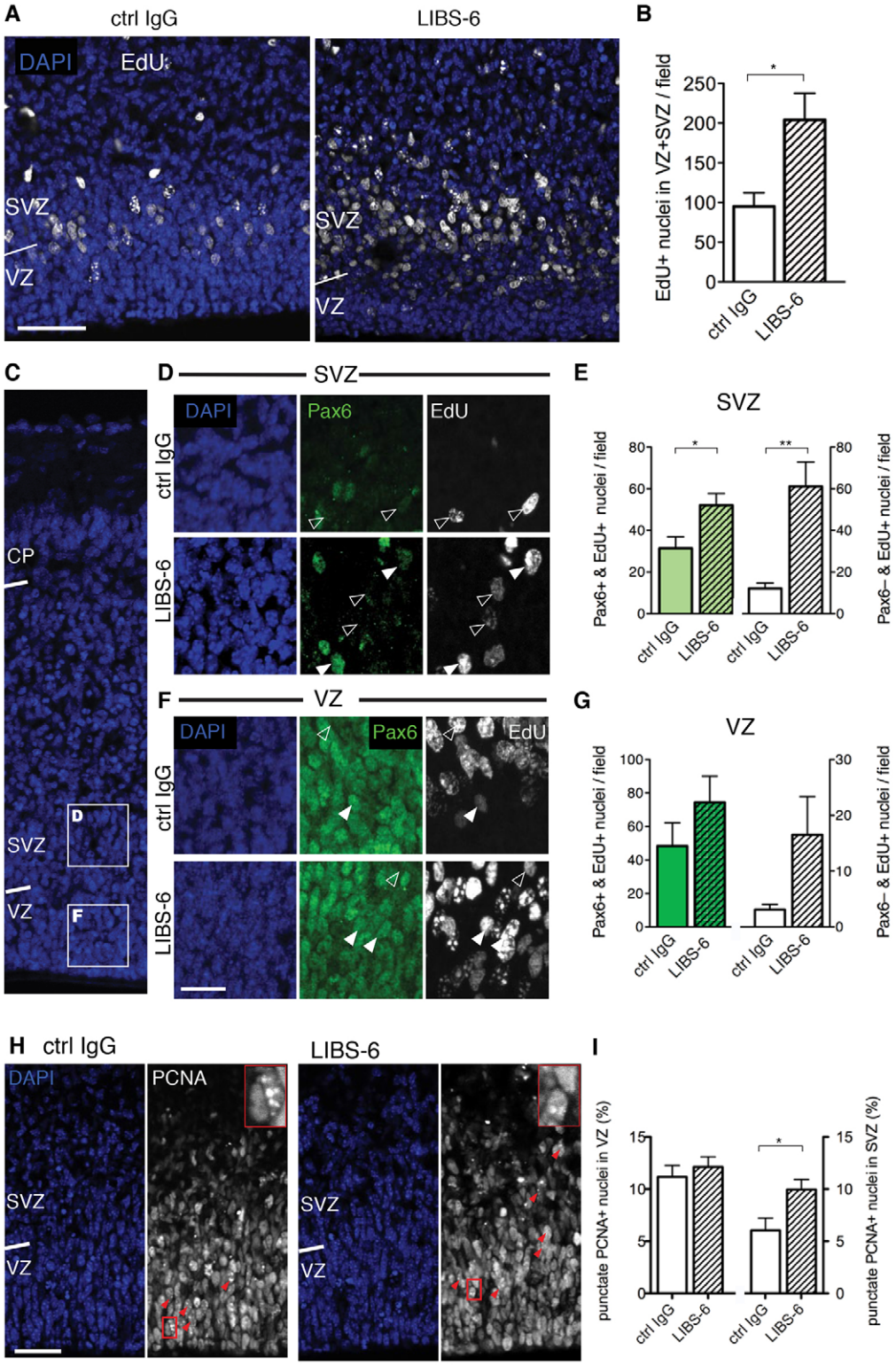

Fig. 2. Itgαvβ3 activation increases cycling progenitors in SVZ. (A-I) 48-hour HERO cultures of E14.5 mouse dorsal telencephalon with ctrl IgG or LIBS-6. (A-G) EdU labeling during the last hour of culture. (A) EdU fluorescence (white) and DAPI staining (blue) (4.05-μm stacks). (B) EdU+ nuclei in VZ plus SVZ per field. (C) Overview of DAPI-stained neocortex. Insets indicate areas of VZ and SVZ (from other sections) shown at higher magnification in F and D, respectively. (D,F) Higher magnification images (4.05-μm stacks) of SVZ (D) and VZ (F) triple-stained for DAPI (blue), Pax6 (green) and EdU (white). Solid arrowheads, Pax6+ EdU+ nuclei; open arrowheads, Pax6– (or very weakly Pax6+) EdU+ nuclei. (E,G) Pax6+ EdU+ nuclei (green columns) and Pax6– EdU+ nuclei (white columns) in VZ (G) and SVZ (E) per field. Note: Immunofluorescence signal for Pax6+ nuclei was relatively weaker in SVZ (light green columns in E) than VZ (dark green columns in G). (B,E,G) Mean of four hemispheres. Fields, 225×225 μm. (H) Proliferating cell nuclear antigen (PCNA) immunofluorescence (white) and DAPI staining (blue) (single 0.74-μm optical sections). Red insets are shown at higher magnification in the top right corners. Red arrowheads, punctate PCNA+ nuclei in S-phase. (I) Punctate PCNA+ nuclei expressed as percentage of all PCNA+ nuclei in VZ (left) and SVZ (right) per radial field. Mean of five to seven hemispheres. Scale bars: 50 μm in A; 20 μm in F; 35 μm in H.

approximately half of the EdU+ progenitors in the SVZ (Fig. 2E), was greater than that in the total BP population as revealed by the abundance of basal mitoses (Fig. 1C). Given the previous finding that proliferating BPs exhibit a twofold longer S-phase than neurogenic BPs (Arai et al., 2011), this raised the possibility that the increase in EdU incorporation may in part reflect a greater relative proportion of S-phase in the BP cell cycle. We investigated this possibility by proliferating cell nuclear antigen (PCNA) immunostaining, which shows a punctate nuclear pattern during S-phase (Fig. 2H). Quantification of punctate PCNA-positive nuclei after 48-hour HERO culture revealed a significant increase in the proportion of nuclei in S-phase in the SVZ, but not VZ, upon LIBS-6 treatment (Fig. 2I). However, the fold-increase was substantially less than that in the Pax6– EdU+ nuclei in the SVZ (Fig. 2E). We therefore conclude that the increase in Pax6– EdU+ SVZ nuclei, i.e. in IPCs/TAPs, upon itgαvβ3 activation that can be accounted for by

Development (2014) doi:10.1242/dev.101907

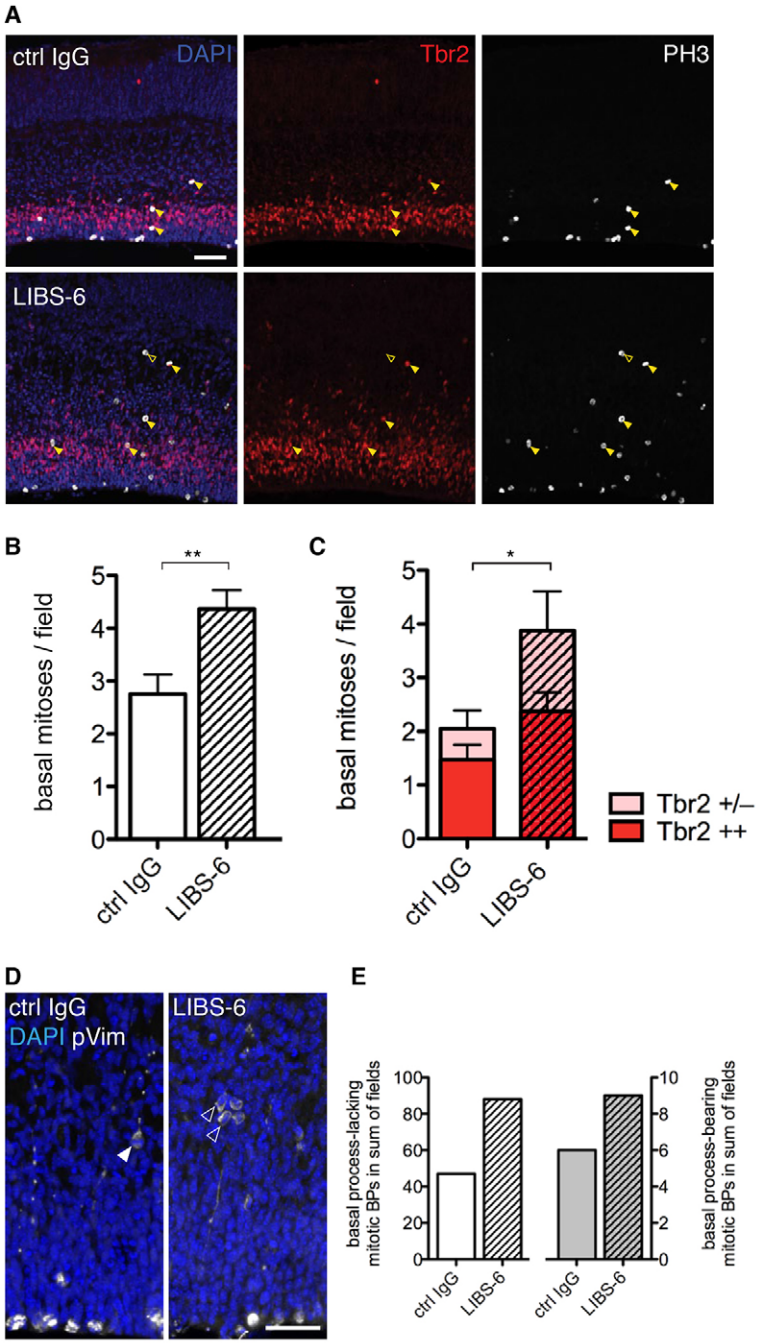

Fig. 3. Itgαvβ3 activation increases mitotic BPs, which are mostly IPCs/TAPs. (A-E) 48-hour HERO cultures of E14.5 mouse dorsal telencephalon with ctrl IgG or LIBS-6. (A) Tbr2 (red) and PH3 (white) immunofluorescence, and DAPI staining (blue) (single 1.91-μm optical sections). Solid arrowheads, Tbr2+ mitotic BPs; open arrowheads, Tbr2– mitotic BP. (B) Basal mitoses per field (250×250 μm). Mean of eight hemispheres. (C) Tbr2+ basal mitoses per field (250×250 μm). Dark red, strongly Tbr2-positive (++) basal mitoses; light red, weakly Tbr2-positive (+) and Tbr2-negative (–) basal mitoses. Mean of six hemispheres. (D) Phosphovimentin immunofluorescence (pVim, white) and DAPI staining (blue) (4.62-μm stacks). Solid arrowhead, mitotic bRGC; open arrowheads, mitotic IPCs/TAPs. (E) Basal process-lacking (left) and basal process-bearing (right) mitotic BPs. Sum of 12 fields (225×225 μm) of 11 hemispheres. Scale bars: 50 μm in A; 35 μm in D.

stimulation of proliferation is actually in accordance with the increase in basal mitoses (Fig. 1C).

Most BP proliferation upon itgαvβ3 activation is due to IPCs/TAPs

To obtain independent evidence showing that the increase in basal mitoses (Fig. 1C) and in EdU+ nuclei in the SVZ (Fig. 2E) upon itgαvβ3 activation indeed reflected an increase in BPs, we performed immunostaining for the BP marker Tbr2 (Eomes – Mouse Genome Informatics) (Englund et al., 2005) (Fig. 3A). As was the case after 24 hours of HERO culture, LIBS-6 treatment in HERO culture for 48 hours significantly increased the number of basal mitoses (Fig. 3B). The vast majority of these were either strongly or weakly Tbr2-positive (Fig. 3C), corroborating our conclusion that itgαvβ3 activation promotes BP proliferation. We noticed that some of the increased basal, Tbr2+ mitoses observed upon LIBS-6 treatment were located in the basal region of the SVZ and in the intermediate zone (Fig. 3A), raising the possibility that itgαvβ3 activation might affect BP migration.

By morphology, mouse mitotic BPs as identified by phosphovimentin staining fall into two principal groups, either possessing (bRGCs) or lacking (IPCs, TAPs) a basal process at mitosis (Reillo et al., 2011; Shitamukai et al., 2011; Wang et al., 2011; Kelava et al., 2012). We therefore performed phosphovimentin immunostaining to determine to which extent the increased BP proliferation observed upon itgαvβ3 activation pertained to IPCs/TAPs versus bRGCs (Fig. 3D). LIBS-6 treatment in HERO culture for 48 hours doubled the number of basal process-lacking mitotic BPs, i.e. IPCs and/or TAPs, which comprised ≈90% of all mitotic BPs (Fig. 3E, left). LIBS-6 treatment also moderately

Development (2014) doi:10.1242/dev.101907

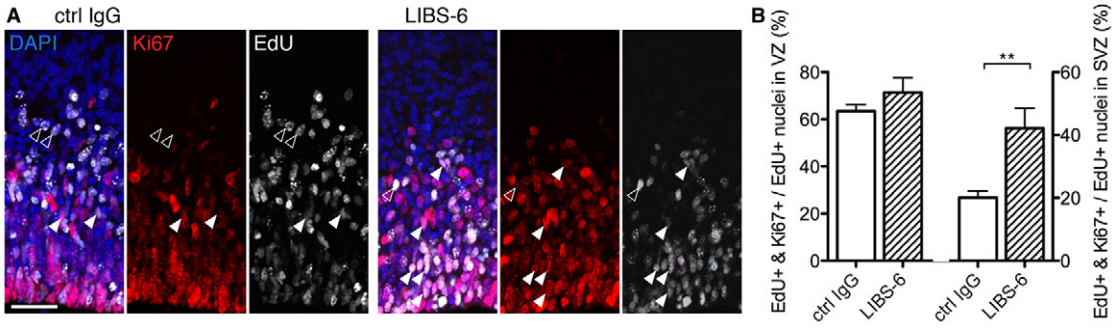

Fig. 4. Itgαvβ3 activation promotes cell cycle re-entry of BPs. (A,B) 49-hour HERO cultures of E14.5 mouse dorsal telencephalon with ctrl IgG or LIBS-6, with EdU labeling for 1 hour after 24 hours of culture. (A) Ki67 immunofluorescence (red), EdU fluorescence (white) and DAPI staining (blue) (single 0.97-µm optical sections). Solid arrowheads, cycling progenitors (EdU+ Ki67+); open arrowheads, cells that exited the cell cycle (EdU+ Ki67–) during the last 24 hours of culture. (B) Cycling progenitors (EdU+ Ki67+ nuclei) expressed as percentage of all EdU+ nuclei in VZ (left) and SVZ (right) per radial field. Mean of four hemispheres. Scale bar: 35 µm.

increased the minor population of basal process-bearing mitotic BPs, i.e. bRGCs (Fig. 3E, right). Thus, the increase in the BP population upon itgαvβ3 activation was mostly due to increased IPC and/or TAP proliferation.

Itgαvβ3 activation promotes BP cell cycle re-entry

IPCs and TAPs differ in the number of rounds of cell division they undergo. IPCs typically undergo only one, self-consuming division that yields two postmitotic neurons, whereas TAPs can re-enter the cell cycle (Haubensak et al., 2004; Miyata et al., 2004; Noctor et al., 2004; Attardo et al., 2008; Noctor et al., 2008; Hansen et al., 2010; Betizeau et al., 2013). We therefore determined whether the increase in BPs upon itgαvβ3 activation reflected an increased capacity of IPCs to re-enter the cell cycle. To this end, we performed, in the presence of either ctrl IgG or LIBS-6, a 1-hour EdU pulse-labeling at the end of a 24-hour HERO culture, followed by another 24-hour HERO culture and analysis of cycling cells by Ki67 immunostaining (Fig. 4A). LIBS-6 treatment increased the proportion of nuclei that were both, EdU+ and Ki67-positive (Ki67+), in the SVZ but not VZ (Fig. 4B). Considering the length of S-, G2- and M-phase of E14.5 BPs (Arai et al., 2011), these data imply that itgαvβ3 activation promoted the cell cycle re-entry of BPs; that is, it induced a portion of IPCs to adopt a TAP-like behavior.

Itgαvβ3 activation decreases the proportion of neurogenic IPCs and promotes symmetric proliferative divisions of cortical progenitors

Tis21 (*Btg2* – Mouse Genome Informatics) is a prodifferentiative gene that among BPs is typically expressed in IPCs undergoing self-consuming symmetric neurogenic division (Haubensak et al., 2004; Attardo et al., 2008). These *Tis21*-expressing IPCs comprise ≈80% of all BPs in the E14.5 mouse neocortex (Arai et al., 2011). Conversely, the ≈20% BPs that lack *Tis21* expression probably correspond to the minor BP subpopulation in embryonic rodent neocortex shown to undergo repeated rounds of cell division (Noctor et al., 2004; Noctor et al., 2008), i.e. displaying a TAP-like behavior, and in addition presumably include at least some self-renewing bRGCs, which in mouse constitute another minor BP subpopulation (Shitamukai et al., 2011; Wang et al., 2011; Kelava et al., 2012). Given these previous observations, one would expect that the itgαvβ3-induced increase in BPs capable of cell cycle re-entry (Fig. 4B) should be accompanied by an increase in BPs lacking *Tis21* expression.

To investigate this hypothesis, we took advantage of a *Tis21*-green fluorescent protein (GFP) knock-in mouse line in which nuclear GFP is expressed under the control of the *Tis21* promoter (Haubensak et al., 2004). LIBS-6 treatment for 48 hours in HERO culture led to a decrease in *Tis21*-GFP-positive (*Tis21*-GFP+) nuclei in both the VZ and SVZ (Fig. 5A-C). Extending these data, double immunofluorescence for Ki67 showed that among the progenitors present in VZ and SVZ, LIBS-6 treatment caused a decrease in the proportion of *Tis21*-GFP+, i.e. neurogenic, progenitors (Fig. 5D,F). Thus, itgαvβ3 activation increased not only the population size of BPs (Fig. 1C, Fig. 2E, Fig. 3B,C,E), but also the proportion of *Tis21*-GFP-negative (*Tis21*-GFP–) progenitors within this population. Accordingly, LIBS-6 treatment increased the percentage of *Tis21*-GFP– mitotic BPs at the expense of *Tis21*-GFP+ mitotic BPs (Fig. 5E,G). In line with the decrease in *Tis21*-GFP+ neurogenic IPCs, LIBS-6 treatment in HERO culture for up to 48 hours did not result in an increased number of neurons per field (supplementary material Fig. S4). Taken together, our data are consistent with the notion that itgαvβ3 activation results in a portion of IPCs switching from a self-consuming, symmetric neurogenic division to amplifying, symmetric proliferative divisions.

To further investigate whether itgαvβ3 activation promotes symmetric proliferative progenitor divisions, we performed experiments with dissociated cells from E14.5 mouse dorsolateral telencephalon in culture. Dissociated cells plated at low density were exposed for 24 hours either to LIBS-6, or to control IgG, followed by Ki67 and Tuj1 double immunofluorescence to identify cycling progenitors and newborn neurons, respectively. At the end of the 24-hour culture period, we scored only pairs of nascent daughter cells; that is, before completion of cytokinesis (i.e. before abscission) (Fig. 6A). Itgαvβ3 activation by LIBS-6 resulted in a significant decrease in the percentage of pairs consisting of two neurons (Fig. 6A,B, N+N) and a corresponding increase in pairs consisting of two progenitors (Fig. 6A,B, P+P), without a change in pairs consisting of one progenitor and one neuron (Fig. 6A,B, P+N). Relating these *in vitro* results to the *in vivo* situation, it should be noted that at E14.5 APs are known to generate neurons typically by asymmetric division, whereas BPs do so by symmetric division (Haubensak et al., 2004; Miyata et al., 2004; Noctor et al., 2004; Attardo et al., 2008; Noctor et al., 2008). Hence, one may interpret the decrease in N+N pairs upon itgαvβ3 activation observed with dissociated cortical cells in culture (Fig. 6B) to reflect a decrease in symmetric neurogenic BP divisions. This in turn would suggest that the increase in P+P pairs upon itgαvβ3 activation may predominantly reflect an increase in symmetric proliferative divisions of BPs.

Development (2014) doi:10.1242/dev.101907

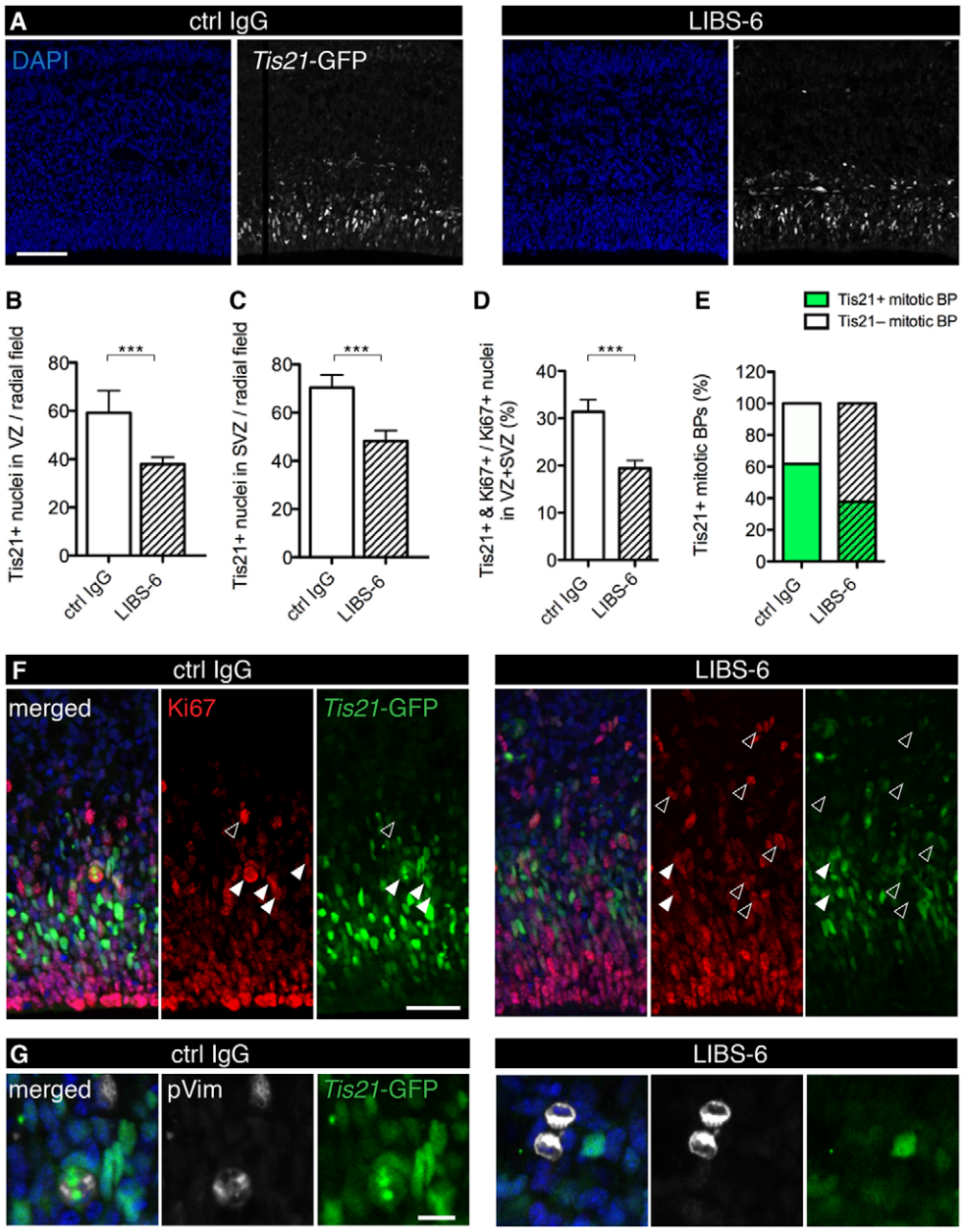

Fig. 5. Itgαvβ3 activation decreases the proportion of neurogenic (*Tis21*-GFP+) BPs. (A-G) 48-hour HERO cultures of E14.5 mouse dorsal telencephalon from *Tis21*-GFP mice with ctrl IgG or LIBS-6. (A) *Tis21*-GFP immunofluorescence (white) and DAPI staining (blue) (single 0.74-µm optical sections). (B,C) *Tis21*-GFP+ cells per radial field in VZ (B) and SVZ (C). Mean of four hemispheres. (D) Progenitors (identified by Ki67 immunofluorescence) that show *Tis21*-GFP expression (Tis21+ Ki67+), expressed as percentage of all progenitors (Ki67+ nuclei) in VZ plus SVZ per radial field. Mean of 11 hemispheres. (E) Percentage of mitotic BPs (abventricular mitoses identified by phosphovimentin immunofluorescence) that show *Tis21*-GFP expression (Tis21+, green). Sum of 29 fields (225×225 µm) from 11 hemispheres. (F) Ki67 (red) and *Tis21*-GFP (green) immunofluorescence, and DAPI staining (blue) (single 0.97-µm optical sections). Solid arrowheads, *Tis21*-GFP+ Ki67+ (neurogenic) progenitors; open arrowheads, *Tis21*-GFP– Ki67+ (proliferative) progenitors. (G) Mitotic BPs in SVZ, identified by phosphovimentin immunofluorescence (white), that either show (left) or lack (right) *Tis21*-GFP expression (green, immunofluorescence) (single 0.97-µm optical sections). Blue, DAPI staining. Scale bars: 50 µm in A; 35 µm in F; 10 µm in G.

Increased BP levels upon itgαvβ3 activation are not due to increased BP generation from APs nor increased AP delamination

Taken together, the effects of LIBS-6 treatment on BPs described so far are best explained by itgαvβ3 activation directly stimulating their proliferation. This conclusion is in accordance with the spatial circumstances concerning the antibody administration, as upon its addition to hemispheres in HERO culture, antibody can be expected to reach delaminated BPs by paracellular diffusion (Aaku-Saraste et al., 1996; Loulier et al., 2009).

Additional evidence in support of the above conclusion comes from considering the effects of LIBS-6 treatment on APs. First, although LIBS-6 treatment for 24 hours increased not only the level of mitotic BPs (Fig. 1C), but also that of mitotic APs (Fig. 1B), the magnitude of the latter increase was less than the former, and the increase in mitotic APs was not accompanied by a statistically significant increase in AP proliferation (Fig. 2G, left) nor in AP cell cycle re-entry (Fig. 4B, left) at 48 hours of HERO culture. Hence, it is very unlikely that the marked increase in BP proliferation (Fig. 2E), mitotic Tbr2+ BPs (Fig. 3C) and BP cell cycle re-entry (Fig. 4B, right) upon itgαvβ3 activation that we observed at 48 hours of HERO culture was the result of an increased BP generation by APs. Second, the increase in mitotic APs observed after 24 hours of LIBS-6 treatment (Fig. 1B) was accompanied by an increase in lateral length (Fig. 1F), which implies an expansion of APs by symmetric proliferative divisions generating two APs each, rather than an increase in AP divisions generating BPs.

Moreover, our findings that the proliferating mitotic BPs observed at higher level upon itgαvβ3 activation expressed the BP marker Tbr2 (Fig. 3C) and downregulated (Fig. 2E, left) or lacked (Fig. 2E, right) the AP marker Pax6 render it highly unlikely that these cells were delaminated APs. Further evidence against this scenario was obtained by experiments interfering with Notch signaling (supplementary material Fig. S5). Thus, neither increased BP generation from APs nor increased AP delamination appear to underlie the increase in cycling BP levels upon itgαvβ3 activation.

Development (2014) doi:10.1242/dev.101907

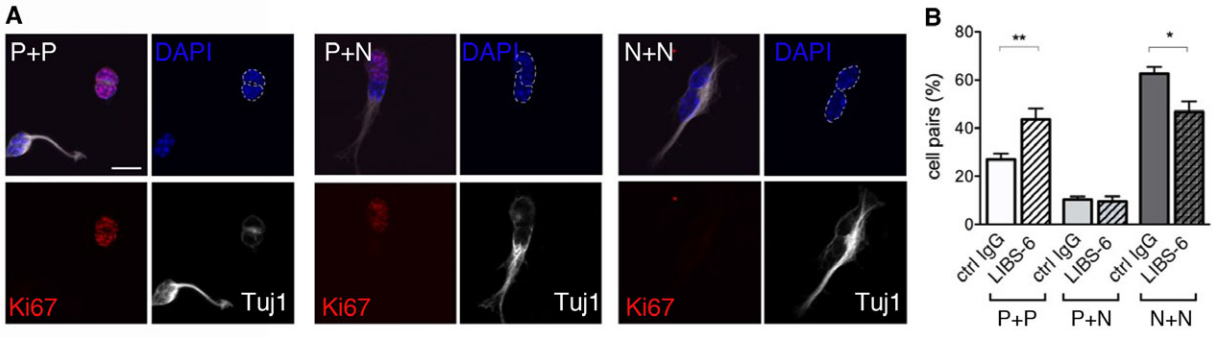

Fig. 6. Itgαvβ3 activation decreases symmetric neurogenic and increases symmetric proliferative divisions of cortical progenitors *in vitro*. (A,B) 24-hour culture of dissociated cells from E14.5 dorsolateral telencephalon with ctrl IgG or LIBS-6. (A) Ki67 (red) and Tuj1 (white) immunofluorescence combined with DAPI staining (blue) of nascent daughter cell pairs (2.3-μm stacks). Note that Tuj1 immunofluorescence images are shown slightly overexposed on purpose, in order to visualize the outline not only of Tuj1+, but also Tuj1– nascent daughter cells. Dashed lines in DAPI images (top right panels) outline nascent daughter cell nuclei. (B) Percentage of symmetric proliferative (P+P), asymmetric self-renewing/neurogenic (P+N) and symmetric neurogenic (N+N) divisions. Five images were acquired per coverslip and average percentage of each type of division was calculated. Mean of six coverslips from two independent experiments. Scale bar: 10 μm. P, progenitors; N, neurons.

This in turn supports our conclusion that this increase is due to activated itgαvβ3 directly stimulating BP proliferation, notably inducing a portion of IPCs to adopt a TAP-like behavior. The exact mechanism by which itgαvβ3 activation leads to this effect, for example whether it involves altered IPC migration (see Fig. 3A), remains to be investigated.

Depletion of thyroid hormones reduces cortical progenitor proliferation

Interestingly, itgαvβ3 is the only known non-nuclear, cell surface receptor of thyroid hormones (THs) (Bergh et al., 2005; Cody et al., 2007). Furthermore, binding of THs to itgαvβ3, like other modes of integrin activation (see supplementary material Fig. S2), results in ERK activation, which in turn leads to cell proliferation (reviewed in Davis et al., 2011). We therefore explored a possible role of THs in the itgαvβ3-induced BP proliferation.

We first examined the physiological role of endogenous THs on cortical progenitor proliferation in general. For this purpose, we turned to rat, an established model system that in contrast to mouse allows efficient pharmacological depletion of thyroid hormones. Specifically, pregnant rats received 2-mercapto-1-methylimidazole (MMI) with the drinking water (Fig. 7A), which prevents the synthesis of THs (Ausó et al., 2004). After 10 days of MMI treatment, pregnant rats were found to be completely deprived of THs compared with control, in contrast to pregnant mice treated with MMI for 14 days (supplementary material Table S2).

Flow cytometry of dissociated cells from the neocortex of E16.5 rats (corresponding to E14.5 mice) showed that, compared with control, the proportion of cycling (PCNA+) cells, i.e. cortical progenitors, was substantially (by 34%) reduced upon TH depletion (Fig. 7B). Analysis of dissociated cortical progenitors for Pax6 and Tbr2 revealed that this reduction concerned both, Pax6+/Tbr2– progenitors, i.e. APs (Fig. 7C), and Tbr2+ progenitors, i.e. BPs (Fig. 7D). In this analysis, we noticed that ≈95% of all cortical progenitors from control rat embryos scored as Pax6+, implying that the majority of the Tbr2+ BPs still contained detectable Pax6 immunoreactivity. By contrast, in the case of MMI-treated rat embryos, Pax6+ progenitors and Tbr2+ progenitors together accounted for essentially all progenitors present, implying that upon TH depletion the majority of the Tbr2+ BPs lacked detectable Pax6 immunoreactivity. This may suggest that THs somehow negatively influence Pax6 downregulation in newborn BPs.

TH depletion reduced the proportion of newborn neurons, as revealed by flow cytometry analysis of dissociated cells from E19.5 rat neocortex for the marker Tbr1 (Fig. 7E). This decrease likely reflected diminished neurogenesis due to the reduced population of APs and BPs caused by the TH deficiency. Together, these data indicate that in normal neocortical development, neural progenitors require the presence of THs to reach their full population size and to generate the complement of neurons (Mohan et al., 2012).

TH binding to itgαvβ3 is required for the LIBS-6–mediated increase in BP proliferation

We next investigated whether the BP proliferation induced by activation of itgαvβ3 using LIBS-6 involved THs. For this purpose, we used tetraiodothyroacetic acid (tetrac), a thyroxin analog that specifically interferes with TH binding to itgαvβ3 and thereby inhibits the TH effects that are transduced by itgαvβ3 (Bergh et al., 2005; Davis et al., 2011). This pharmacological agent appears to be the most specific tool presently at hand to investigate a potential role of THs in the itgαvβ3-mediated stimulation of BP proliferation. To our knowledge, no itgαvβ3 mutants have been reported to date that selectively abrogate the binding of THs, but not ECM ligands, to itgαvβ3.

To address the *in vivo* relevance of itgαvβ3-TH interaction, we administered tetrac by intraventricular injection into mouse embryos *in utero* (Fig. 7F). We first established the validity of this approach by confirming that intraventricular injection of LIBS-6 (at fourfold higher concentration than for HERO culture to account for the estimated dilution by the ventricular fluid) exerted the same effect on cortical progenitor proliferation *in vivo* as in HERO culture. Antibodies injected intraventricularly into E14.5 mouse embryos *in utero* have previously been shown to reach the cortical SVZ by paracellular diffusion (Loulier et al., 2009), consistent with the absence of tight junctions after neural tube closure (Aaku-Saraste et al., 1996). Indeed, intraventricular LIBS-6 injection at E14.5 resulted in an increase in mitotic APs and, even more so, in mitotic BPs 24 hours later (Fig. 7G-I, blue).

In the absence of targeted itgαvβ3 activation by LIBS-6, inhibition of endogenous TH binding to itgαvβ3 by intraventricular injection of tetrac significantly reduced the physiological level of mitotic APs, but not that of mitotic BPs (Fig. 7G-I, red). These data show that THs sustain AP proliferation via itgαvβ3 in embryonic mouse neocortex. In fact, under the present experimental conditions,

Development (2014) doi:10.1242/dev.101907

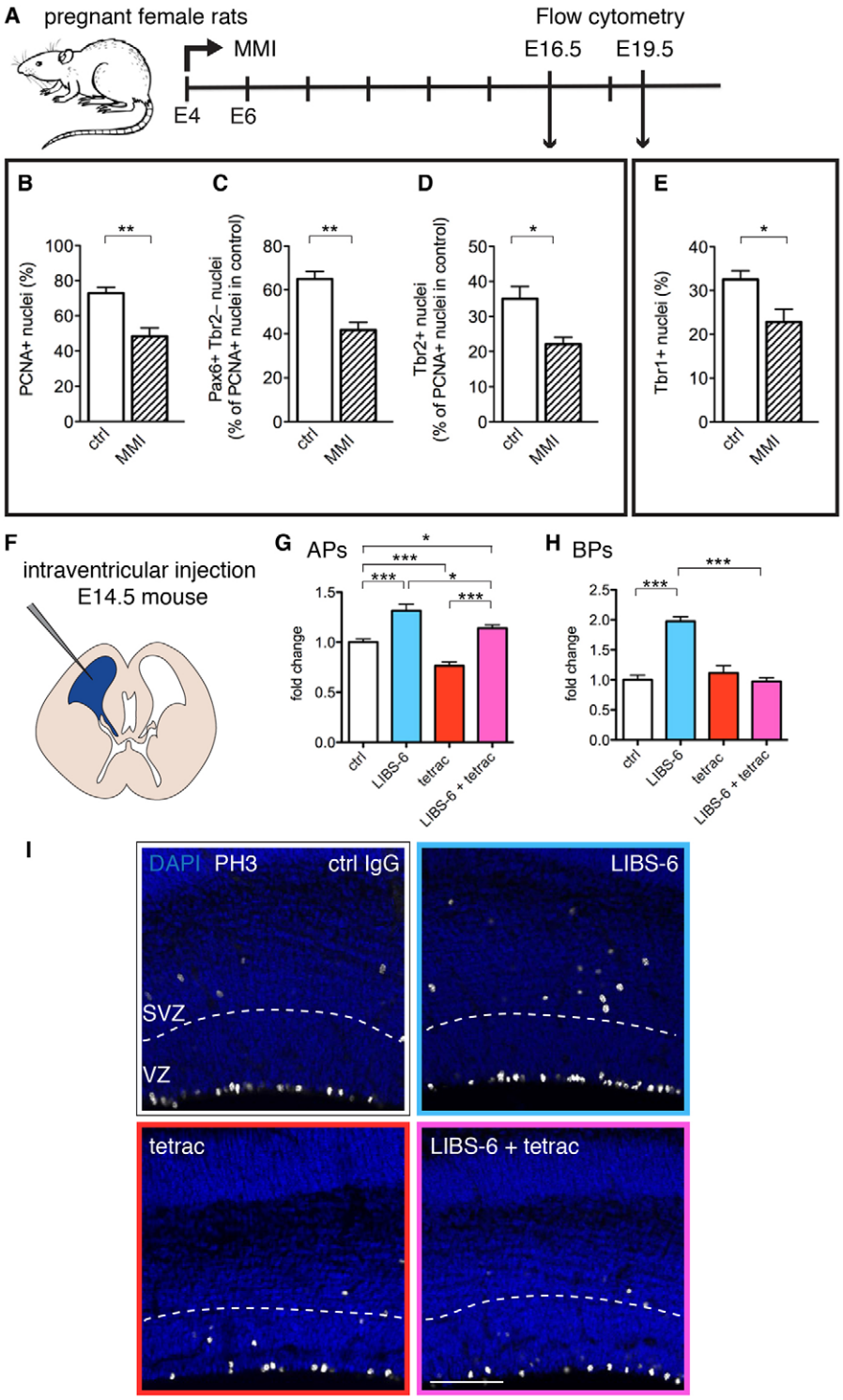

Fig. 7. THs promote the proliferation of cortical progenitors, notably BPs, via itgαvβ3. (A) Embryos from control (ctrl) and TH-depleted (MMI-treatment starting at E4 or E6) pregnant rats were analyzed at E16.5 or E19.5. Neocortices were dissociated, cortical cells were fixed, subjected to immunofluorescence for PCNA and either Pax6 or Tbr2 (B-D), or for Tbr1 (E), combined with propidium iodide staining, and analyzed by flow cytometry. (B) PCNA+ nuclei expressed as percentage of all nuclei at E16.5. (C) Pax6+ Tbr2– nuclei expressed as percentage of all PCNA+ nuclei in control at E16.5. Note that in control, 95% of all PCNA+ nuclei were Pax6+. As also 35% of all PCNA+ nuclei were Tbr2+ (see D), at least 30% of all PCNA+ nuclei in the control must be Pax6+ and Tbr2+, i.e. BPs. Consequently, this value was subtracted from the 95% value for Pax6+ nuclei, yielding the 65% value for Pax6+ Tbr2– nuclei shown in C. (D) Tbr2+ nuclei expressed as percentage of all PCNA+ nuclei in control at E16.5. Note that in contrast to control, Tbr2+ BPs from MMI-treated neocortex lacked Pax6 immunoreactivity. (E) Tbr1+ nuclei expressed as percentage of all nuclei at E19.5. (B-E) Mean of three cell suspensions, each obtained from three or more hemispheres. (F-I) TH displacement from itgαvβ3 by intraventricular injection of tetrac into mouse embryos *in utero*. E14.5 mice were injected with ctrl IgG or control saline (ctrl, *n*=8), LIBS-6 (*n*=5), tetrac (*n*=4), or LIBS-6+tetrac (*n*=7) and analyzed after 24 hours of *in utero* development. (F) Cartoon of intraventricular injection. (G,H) Mitotic APs (G) and BPs (H) in ctrl (white), LIBS-6 (blue), tetrac (red) and LIBS-6+tetrac (purple) -injected neocortex per field (225×225 µm), expressed as fold change relative to ctrl. Mean of four to eight injected embryos. (I) PH3 immunofluorescence (white) and DAPI staining (blue) (single 0.74 µm optical sections) of ctrl IgG, LIBS-6, tetrac and LIBS-6+tetrac-injected neocortex. Dashed lines, boundary of VZ and SVZ. Scale bar: 50 µm.

tetrac would be expected to affect only the level of mitotic APs, but not that of mitotic BPs, for two reasons. First, in mouse, APs, but not the vast majority of BPs, undergo repeated cell divisions (Fietz and Huttner, 2011; Lui et al., 2011; Borrell and Reillo, 2012), and hence only APs should be susceptible to proliferation inhibitors. Second, in light of the cell cycle length of E14.5 APs (≈19 hours) and BPs (≈26 hours) (Arai et al., 2011), one would not expect the reduced level of mitotic APs observed after 24 hours of tetrac administration (Fig. 7G, red) to already yield a detectable reduction in the level of mitotic BPs. Our data are consistent with the notion that the intrinsic self-renewal capacity of APs involves constitutive itgαvβ3 activation by ECM (Arai et al., 2011) that is sustained by TH binding to itgαvβ3. By contrast, mouse BPs appear to lack this constitutive itgαvβ3 activation, presumably owing to the lack of endogenous ECM production (Arai et al., 2011) (supplementary material Fig. S6).

Remarkably, intraventricular injection of tetrac completely blocked the increase in mitotic BPs elicited upon targeted itgαvβ3 activation by LIBS-6 (Fig. 7H,I, purple versus blue). Thus, when BPs are induced to proliferate by itgαvβ3 activation, this requires

Development (2014) doi:10.1242/dev.101907

the simultaneous presence of THs. By contrast, tetrac only partially abrogated the increase in mitotic APs elicited by LIBS-6 administration (Fig. 7G,I, purple versus blue), and thus LIBS-6 treatment in the presence of tetrac still caused an increase in mitotic APs (Fig. 7G,I, purple versus red). In other words, only the constitutive proliferation of APs (Fig. 7G,I, white versus red), but not that elicited by LIBS-6-mediated itgαvβ3 activation (Fig. 7G,I, compare blue versus white with purple versus red), appears to be sensitive to TH displacement from itgαvβ3.

We conclude that mouse BPs differ from APs with regard to the need of TH binding to itgαvβ3 in order to sustain the proliferation induced by the targeted activation of this integrin by LIBS-6. Whereas BPs are dependent on this hormone-integrin interaction, APs are not. It is tempting to relate this to the differences between mouse BPs and APs with regard to endogenous ECM production and constitutive proliferative capacity. Whereas APs are endowed with both, BPs are not. Thus, we hypothesize that in the case of APs, itgαvβ3 – even upon TH displacement – can still be activated by LIBS-6 to increase progenitor proliferation because of its constitutive interaction with local ECM ligands (supplementary material Fig. S6). In this context, it is interesting to note that: (1) ECM constituents occur abundantly in embryonic ventricular fluid (Zappaterra et al., 2007); (2) APs extend their primary cilium, a sensory organelle, into this fluid (Lehtinen and Walsh, 2011; Louvi and Grove, 2011); and (3) integrins can localize to the ciliary membrane (Seeger-Nukpezah and Golemis, 2012). By contrast, in the case of mouse BPs, there is no such constitutive ECM-itgαvβ3 interaction, rendering its activation by LIBS-6 dependent on the binding of the other principal class of ligands – THs (supplementary material Fig. S6).

DISCUSSION

THs are well-known stimulators of cell proliferation (Sirakov et al., 2012), including neural progenitors (Mohan et al., 2012). The present study contributes the key finding that the stimulation of neural progenitor proliferation by THs is mediated by the TH cell surface receptor itgαvβ3. This is even more significant in light of our findings that mouse BPs, which largely lack self-renewal capacity, are induced to proliferate upon targeted itgαvβ3 activation. The capacity of BPs for proliferation and self-renewal is thought to be a major factor in the evolutionary expansion of the neocortex (Fietz and Huttner, 2011; Lui et al., 2011; Borrell and Reillo, 2012). Thus, itgαvβ3 emerges as a prime candidate to have a key role in this expansion.

We previously showed that in species in which BPs are endowed with self-renewal capacity, such as the gyrencephalic ferret, inhibition of itgαvβ3 signaling reduces the population size of these progenitors (Fietz et al., 2010). Importantly however, aside from APs (Loulier et al., 2009; Radakovits et al., 2009), a link between progenitor self-renewal and integrin signaling has so far only been reported for those BPs that extend a basal process to the basal lamina and that are thought to contact integrin-activating ECM ligands via this process, that is bRGCs (Fietz et al., 2010). We now demonstrate that activation of itgαvβ3 can be sufficient to induce BP proliferation, even in the case of those BPs that do not extend a basal process and for which the molecular basis underlying their proliferative potential has been enigmatic. Thus, our study provides the first evidence that proliferation of basal process-lacking, self-amplifying BPs (i.e. TAPs), which is a characteristic feature of developing human, but not mouse, neocortex and which has been proposed to be linked to the greater BP-autonomous ECM production in human than mouse (Fietz et al., 2012), can indeed be induced by itgαvβ3 activation. Moreover, our study offers a novel, progenitor-based explanation for neurological cretinism; that is, the profound neurological impairment and mental retardation due to defective neocortex development in humans observed upon maternal hypothyroidism or the lack of iodine intake during pregnancy.

MATERIALS AND METHODS

Animals

All animal studies were conducted in accordance with the German animal welfare legislation and guidelines. C57Bl/6, heterozygous *Tis21*-GFP knock-in (Haubensak et al., 2004) and heterozygous Tg(Eomes::GFP) bacterial artificial chromosome (BAC) transgenic (Gong et al., 2003; Kwon and Hadjantonakis, 2007) mice were used at E14.5.

HERO culture

Mouse telencephalic hemispheres were cultured as described (Schenk et al., 2009). Hemispheres received medium containing: (1) 500 µM $MnCl_2$, or an equivalent volume of water; (2) 50 µg/ml LIBS-6 [ligand-induced binding site 6, 2-5 mg/ml stock in phosphate-buffered saline (PBS)], a mouse monoclonal Fab that binds to integrin β3 (Frelinger et al., 1991), or 50 µg/ml mouse isotype control IgG (5 mg/ml stock, Abcam, ab37355); (3) 10 µM *N*-[*N*-(3,5-Difluorophenacetyl-L-alanyl)]-(*S*)-phenylglycine *t*-butyl ester (DAPT) (Calbiochem 565770) dissolved in dimethyl sulfoxide (DMSO) (40 mM stock), or an equivalent volume of DMSO only.

EdU labeling

HERO cultures received 1 mg/ml EdU (Invitrogen) for 1 hour. EdU labeling was performed at the end of a 48-hour culture followed by fixation. Alternatively, EdU labeling was performed after a 24-hour culture, hemispheres transferred to fresh medium, and HERO culture continued for additional 24 hours, followed by fixation.

Microinjection into APs in slice culture

Microinjection of fluorescently labeled dextran (Dx-A594, Invitrogen) in slices of mouse telencephalon was performed as described (Taverna et al., 2011).

Intraventricular injection

For details of *in utero* manipulation and intraventricular injection, see Saito and Nakatsuji (Saito and Nakatsuji, 2001; De Pietri Tonelli et al., 2006; Loulier et al., 2009). The following agents (1-2 µl injected volume) were injected: (1) 0.2 mg/ml LIBS-6 or mouse isotype control IgG in PBS; (2) 200 µM 3,3′,5,5′-tetraiodothyroacetic acid (tetrac, Sigma T3787), from a 100 mM stock in 0.1 N NaOH diluted in PBS, or an equivalent volume of PBS containing 0.2% 0.1 N NaOH only. Intraventricularly injected E14.5 embryos were allowed to develop for 24 hours *in utero*, followed by dissection of brains and fixation.

Nascent daughter cell pair analysis

Three-to-five dorsolateral telencephala were pooled and dissociated using the Neural Tissue Dissociation Kit (papain-based, Miltenyi Biotec) according to the manufacturer's instruction. Cells were grown on poly-D-lysine-coated coverslips at low density (50,000 cells per 1-cm coverslip) in Dulbecco's modified Eagle medium (DMEM) GlutaMax supplemented with 10% fetal calf serum (FCS) and 1% penicillin/streptomycin in presence of 50 µg/ml LIBS-6 or 50 µg/ml mouse isotype control IgG for 24 hours, followed by fixation.

Flow cytometry

Pregnant Sprague-Dawley (JANVIER) rats received 0.02% 2-mercapto-1-methylimidazole (MMI, Sigma 301507) together with 0.3% saccharin, or 0.3% saccharin only (control), with the drinking water, freshly made daily, from gestation day E4 or E6 onwards and were sacrificed at E16.5 or E19.5. PCNA, Pax6, Tbr2 and Tbr1 immunofluorescence was performed on dissociated, paraformaldehyde-fixed, Triton X-100-permeabilized cells of dorsolateral telencephalon according to standard procedures, followed by

flow cytometry (FACSCalibur, BD Bioscience). Data analyses were performed using FlowJo software.

Fluorescence analyses

Hemispheres after HERO culture, intraventricularly injected brains as well as brains dissected from E14.5 C57Bl/6 or Tg(Eomes::GFP) mice, and microinjected brain slices were fixed in 4% paraformaldehyde (PFA) in 120 mM phosphate buffer pH 7.4 overnight at 4°C. Dissociated cortical cells in culture were PFA-fixed for 10 minutes at room temperature.

Fixed hemispheres, and fixed brains from E14.5 C57Bl/6 or Tg(Eomes::GFP)mice, were used for the preparation of 14-µm sagittal cryosections and coronal cryosections, respectively (Kelava et al., 2012). Intraventricularly injected fixed brains, and microinjected fixed brain slices, were used for the preparation of 70 µm and 50 µm, respectively, coronal vibratome sections (Kelava et al., 2012).

Cryosections and vibratome sections, as well as fixed cell cultures, were subjected to immunohistochemistry as described (Fietz et al., 2010; Arai et al., 2011; Kelava et al., 2012). For details on antibodies used, see supplementary material Table S1. Detection of EdU was performed as described (Arai et al., 2011), using the Click-iT Alexa 647 Imaging Kit (Invitrogen, Molecular Probes).

Correlative light and electron microscopy

Performed as described previously (Paridaen et al., 2013). For details see supplementary material Fig. S1.

Immunoblotting

ERK immunoblotting was performed according to standard procedures.

Determination of thyroid hormones in serum

The serum levels of thyroxine and triiodothyronine were determined by radioimmunoassay as previously described (Friedrichsen et al., 2003) (supplementary material Table S2).

Image acquisition and analysis

Confocal images were acquired using a Zeiss LSM DuoScan equipped with 10x, 20x, 25x or 40x objectives. Further image analyses were performed using Fiji software (http://pacific.mpi-cbg.de).

Quantification and statistics

The boundary between VZ and SVZ and beginning of CP were deduced from the orientation and density of nuclei (for details see (Kelava et al., 2012)). Lateral length of cortical wall was determined by measuring the apical, ventricular surface length. Cortical thickness was determined by measuring radial thickness from the apical (i.e. ventricular) to the basal (i.e. pial) side. For determination of radial thickness of the various cortical zones, their boundaries were deduced from the orientation and density of nuclei within these zones. Mitoses at the ventricular surface and within three nuclear diameters from it were considered to be mitotic APs. All other abventricular mitoses in the VZ, SVZ and intermediate zone were considered to be mitotic BPs. Radial field was defined as field over 100 µm of ventricular surface length.

Quantification of phosphoERK immunoblots was performed with ImageJ. Prism software (GraphPad Software) was used for data calculation and illustration. Statistical analyses were performed using two-tailed, unpaired *t*-tests. Error bars in Figs 1-7 indicate s.e.m. * $P \leq 0.05$, ** $P \leq 0.01$, *** $P \leq 0.001$.

Acknowledgements

We are indebted to Mark Ginsberg at the University of California, San Diego, who kindly provided the LIBS-6 antibody. We thank the Animal, Light Microscopy, and FACS Facilities of MPI-CBG for outstanding support, notably Jussi Helppi and team, Jan Peychl and Ina Nüsslein; Iva Kelava for kindly providing the cartoons and for helpful discussion; and Alexander Sykes for helpful discussion and advice on flow cytometry. F.K.W. is a member of the IMPRS for Cell, Developmental and Systems Biology, and a doctoral student at the TU Dresden.

Competing interests

The authors declare no competing financial interests.

Author contributions

D.S. designed and performed the experiments, analyzed the data and wrote the manuscript. M.W.-B. performed correlative light microscopy and electron microscopy and analyzed the data. F.K.W. performed microinjection. H.H. determined thyroid hormone serum concentration and provided advice on the integrin $\alpha_v\beta_3$-thyroid hormone interaction. W.B.H. supervised the project and wrote the manuscript.

Funding

W.B.H. was supported by grants from the Deutsche Forschungsgemeinschaft (DFG) [SFB 655, A2; TRR 83, Tp6] and the European Research Council (ERC) [250197], by the DFG-funded CRTD, and by the Fonds der Chemischen Industrie.

Supplementary material

Supplementary material available online at
http://dev.biologists.org/lookup/suppl/doi:10.1242/dev.101907/-/DC1

References

Aaku-Saraste, E., Hellwig, A. and Huttner, W. B. (1996). Loss of occludin and functional tight junctions, but not ZO-1, during neural tube closure – remodeling of the neuroepithelium prior to neurogenesis. *Dev. Biol.* **180**, 664-679.

Afshari, F. T., Kwok, J. C., Andrews, M. R., Blits, B., Martin, K. R., Faissner, A., Ffrench-Constant, C. and Fawcett, J. W. (2010). Integrin activation or alpha 9 expression allows retinal pigmented epithelial cell adhesion on Bruch's membrane in wet age-related macular degeneration. *Brain* **133**, 448-464.

Arai, Y., Pulvers, J. N., Haffner, C., Schilling, B., Nüsslein, I., Calegari, F. and Huttner, W. B. (2011). Neural stem and progenitor cells shorten S-phase on commitment to neuron production. *Nat. Commun.* **2**, 154.

Attardo, A., Calegari, F., Haubensak, W., Wilsch-Bräuninger, M. and Huttner, W. B. (2008). Live imaging at the onset of cortical neurogenesis reveals differential appearance of the neuronal phenotype in apical versus basal progenitor progeny. *PLoS ONE* **3**, e2388.

Ausó, E., Lavado-Autric, R., Cuevas, E., Del Rey, F. E., Morreale De Escobar, G. and Berbel, P. (2004). A moderate and transient deficiency of maternal thyroid function at the beginning of fetal neocorticogenesis alters neuronal migration. *Endocrinology* **145**, 4037-4047.

Bergh, J. J., Lin, H. Y., Lansing, L., Mohamed, S. N., Davis, F. B., Mousa, S. and Davis, P. J. (2005). Integrin alphaVbeta3 contains a cell surface receptor site for thyroid hormone that is linked to activation of mitogen-activated protein kinase and induction of angiogenesis. *Endocrinology* **146**, 2864-2871.

Betizeau, M., Cortay, V., Patti, D., Pfister, S., Gautier, E., Bellemin-Ménard, A., Afanassieff, M., Huissoud, C., Douglas, R. J., Kennedy, H. et al. (2013). Precursor diversity and complexity of lineage relationships in the outer subventricular zone of the primate. *Neuron* **80**, 442-457.

Borrell, V. and Reillo, I. (2012). Emerging roles of neural stem cells in cerebral cortex development and evolution. *Dev. Neurobiol.* **72**, 955-971.

Cluzel, C., Saltel, F., Lussi, J., Paulhe, F., Imhof, B. A. and Wehrle-Haller, B. (2005). The mechanisms and dynamics of (alpha)v(beta)3 integrin clustering in living cells. *J. Cell Biol.* **171**, 383-392.

Cody, V., Davis, P. J. and Davis, F. B. (2007). Molecular modeling of the thyroid hormone interactions with alpha v beta 3 integrin. *Steroids* **72**, 165-170.

Davis, P. J., Davis, F. B., Mousa, S. A., Luidens, M. K. and Lin, H. Y. (2011). Membrane receptor for thyroid hormone: physiologic and pharmacologic implications. *Annu. Rev. Pharmacol. Toxicol.* **51**, 99-115.

De Pietri Tonelli, D., Calegari, F., Fei, J. F., Nomura, T., Osumi, N., Heisenberg, C. P. and Huttner, W. B. (2006). Single-cell detection of microRNAs in developing vertebrate embryos after acute administration of a dual-fluorescence reporter/sensor plasmid. *Biotechniques* **41**, 727-732.

Dubreuil, V., Marzesco, A. M., Corbeil, D., Huttner, W. B. and Wilsch-Bräuninger, M. (2007). Midbody and primary cilium of neural progenitors release extracellular membrane particles enriched in the stem cell marker prominin-1. *J. Cell Biol.* **176**, 483-495.

Englund, C., Fink, A., Lau, C., Pham, D., Daza, R. A., Bulfone, A., Kowalczyk, T. and Hevner, R. F. (2005). Pax6, Tbr2, and Tbr1 are expressed sequentially by radial glia, intermediate progenitor cells, and postmitotic neurons in developing neocortex. *J. Neurosci.* **25**, 247-251.

Fietz, S. A. and Huttner, W. B. (2011). Cortical progenitor expansion, self-renewal and neurogenesis-a polarized perspective. *Curr. Opin. Neurobiol.* **21**, 23-35.

Fietz, S. A., Kelava, I., Vogt, J., Wilsch-Bräuninger, M., Stenzel, D., Fish, J. L., Corbeil, D., Riehn, A., Distler, W., Nitsch, R. et al. (2010). OSVZ progenitors of human and ferret neocortex are epithelial-like and expand by integrin signaling. *Nat. Neurosci.* **13**, 690-699.

Fietz, S. A., Lachmann, R., Brandl, H., Kircher, M., Samusik, N., Schröder, R., Lakshmanaperumal, N., Henry, I., Vogt, J., Riehn, A. et al. (2012). Transcriptomes of germinal zones of human and mouse fetal neocortex suggest a role of extracellular matrix in progenitor self-renewal. *Proc. Natl. Acad. Sci. USA* **109**, 11836-11841.

Fish, J. L., Dehay, C., Kennedy, H. and Huttner, W. B. (2008). Making bigger brains-the evolution of neural-progenitor-cell division. *J. Cell Sci.* **121**, 2783-2793.

Franco, S. J. and Müller, U. (2013). Shaping our minds: stem and progenitor cell diversity in the mammalian neocortex. *Neuron* **77**, 19-34.

Frelinger, A. L., III, Du, X. P., Plow, E. F. and Ginsberg, M. H. (1991). Monoclonal antibodies to ligand-occupied conformers of integrin alpha IIb beta 3 (glycoprotein IIb-IIIa) alter receptor affinity, specificity, and function. *J. Biol. Chem.* **266**, 17106-17111.

Friedrichsen, S., Christ, S., Heuer, H., Schäfer, M. K., Mansouri, A., Bauer, K. and Visser, T. J. (2003). Regulation of iodothyronine deiodinases in the Pax8-/- mouse model of congenital hypothyroidism. *Endocrinology* **144**, 777-784.

Gong, S., Zheng, C., Doughty, M. L., Losos, K., Didkovsky, N., Schambra, U. B., Nowak, N. J., Joyner, A., Leblanc, G., Hatten, M. E. et al. (2003). A gene expression atlas of the central nervous system based on bacterial artificial chromosomes. *Nature* **425**, 917-925.

Götz, M. and Huttner, W. B. (2005). The cell biology of neurogenesis. *Nat. Rev. Mol. Cell Biol.* **6**, 777-788.

Hansen, D. V., Lui, J. H., Parker, P. R. and Kriegstein, A. R. (2010). Neurogenic radial glia in the outer subventricular zone of human neocortex. *Nature* **464**, 554-561.

Haubensak, W., Attardo, A., Denk, W. and Huttner, W. B. (2004). Neurons arise in the basal neuroepithelium of the early mammalian telencephalon: a major site of neurogenesis. *Proc. Natl. Acad. Sci. USA* **101**, 3196-3201.

Haubst, N., Georges-Labouesse, E., De Arcangelis, A., Mayer, U. and Götz, M. (2006). Basement membrane attachment is dispensable for radial glial cell fate and for proliferation, but affects positioning of neuronal subtypes. *Development* **133**, 3245-3254.

Hynes, R. O. (2002). Integrins: bidirectional, allosteric signaling machines. *Cell* **110**, 673-687.

Imayoshi, I., Sakamoto, M., Yamaguchi, M., Mori, K. and Kageyama, R. (2010). Essential roles of Notch signaling in maintenance of neural stem cells in developing and adult brains. *J. Neurosci.* **30**, 3489-3498.

Kelava, I., Reillo, I., Murayama, A. Y., Kalinka, A. T., Stenzel, D., Tomancak, P., Matsuzaki, F., Lebrand, C., Sasaki, E., Schwamborn, J. C. et al. (2012). Abundant occurrence of basal radial glia in the subventricular zone of embryonic neocortex of a lissencephalic primate, the common marmoset Callithrix jacchus. *Cereb. Cortex* **22**, 469-481.

Konno, D., Shioi, G., Shitamukai, A., Mori, A., Kiyonari, H., Miyata, T. and Matsuzaki, F. (2008). Neuroepithelial progenitors undergo LGN-dependent planar divisions to maintain self-renewability during mammalian neurogenesis. *Nat. Cell Biol.* **10**, 93-101.

Kosodo, Y. and Huttner, W. B. (2009). Basal process and cell divisions of neural progenitors in the developing brain. *Dev. Growth Differ.* **51**, 251-261.

Kriegstein, A. and Alvarez-Buylla, A. (2009). The glial nature of embryonic and adult neural stem cells. *Annu. Rev. Neurosci.* **32**, 149-184.

Kriegstein, A., Noctor, S. and Martínez-Cerdeño, V. (2006). Patterns of neural stem and progenitor cell division may underlie evolutionary cortical expansion. *Nat. Rev. Neurosci.* **7**, 883-890.

Kwon, G. S. and Hadjantonakis, A. K. (2007). Eomes:GFP-a tool for live imaging cells of the trophoblast, primitive streak, and telencephalon in the mouse embryo. *Genesis* **45**, 208-217.

Lathia, J. D., Patton, B., Eckley, D. M., Magnus, T., Mughal, M. R., Sasaki, T., Caldwell, M. A., Rao, M. S., Mattson, M. P. and ffrench-Constant, C. (2007). Patterns of laminins and integrins in the embryonic ventricular zone of the CNS. *J. Comp. Neurol.* **505**, 630-643.

Lehtinen, M. K. and Walsh, C. A. (2011). Neurogenesis at the brain-cerebrospinal fluid interface. *Annu. Rev. Cell Dev. Biol.* **27**, 653-679.

Loulier, K., Lathia, J. D., Marthiens, V., Relucio, J., Mughal, M. R., Tang, S. C., Coksaygan, T., Hall, P. E., Chigurupati, S., Patton, B. et al. (2009). beta1 integrin maintains integrity of the embryonic neocortical stem cell niche. *PLoS Biol.* **7**, e1000176.

Louvi, A. and Grove, E. A. (2011). Cilia in the CNS: the quiet organelle claims center stage. *Neuron* **69**, 1046-1060.

Lui, J. H., Hansen, D. V. and Kriegstein, A. R. (2011). Development and evolution of the human neocortex. *Cell* **146**, 18-36.

Miyata, T., Kawaguchi, A., Saito, K., Kawano, M., Muto, T. and Ogawa, M. (2004). Asymmetric production of surface-dividing and non-surface-dividing cortical progenitor cells. *Development* **131**, 3133-3145.

Mohan, V., Sinha, R. A., Pathak, A., Rastogi, L., Kumar, P., Pal, A. and Godbole, M. M. (2012). Maternal thyroid hormone deficiency affects the fetal neocorticogenesis by reducing the proliferating pool, rate of neurogenesis and indirect neurogenesis. *Exp. Neurol.* **237**, 477-488.

Noctor, S. C., Martínez-Cerdeño, V., Ivic, L. and Kriegstein, A. R. (2004). Cortical neurons arise in symmetric and asymmetric division zones and migrate through specific phases. *Nat. Neurosci.* **7**, 136-144.

Noctor, S. C., Martínez-Cerdeño, V. and Kriegstein, A. R. (2008). Distinct behaviors of neural stem and progenitor cells underlie cortical neurogenesis. *J. Comp. Neurol.* **508**, 28-44.

Osumi, N., Shinohara, H., Numayama-Tsuruta, K. and Maekawa, M. (2008). Concise review: Pax6 transcription factor contributes to both embryonic and adult neurogenesis as a multifunctional regulator. *Stem Cells* **26**, 1663-1672.

Paridaen, J. T., Wilsch-Bräuninger, M. and Huttner, W. B. (2013). Asymmetric inheritance of centrosome-associated primary cilium membrane directs ciliogenesis after cell division. *Cell* **155**, 333-344.

Pontious, A., Kowalczyk, T., Englund, C. and Hevner, R. F. (2008). Role of intermediate progenitor cells in cerebral cortex development. *Dev. Neurosci.* **30**, 24-32.

Pucilowska, J., Puzerey, P. A., Karlo, J. C., Galán, R. F. and Landreth, G. E. (2012). Disrupted ERK signaling during cortical development leads to abnormal progenitor proliferation, neuronal and network excitability and behavior, modeling human neuro-cardio-facial-cutaneous and related syndromes. *J. Neurosci.* **32**, 8663-8677.

Radakovits, R., Barros, C. S., Belvindrah, R., Patton, B. and Müller, U. (2009). Regulation of radial glial survival by signals from the meninges. *J. Neurosci.* **29**, 7694-7705.

Rakic, P. (2009). Evolution of the neocortex: a perspective from developmental biology. *Nat. Rev. Neurosci.* **10**, 724-735.

Reillo, I., de Juan Romero, C., García-Cabezas, M. A. and Borrell, V. (2011). A role for intermediate radial glia in the tangential expansion of the mammalian cerebral cortex. *Cereb. Cortex* **21**, 1674-1694.

Saito, T. and Nakatsuji, N. (2001). Efficient gene transfer into the embryonic mouse brain using in vivo electroporation. *Dev. Biol.* **240**, 237-246.

Schenk, J., Wilsch-Bräuninger, M., Calegari, F. and Huttner, W. B. (2009). Myosin II is required for interkinetic nuclear migration of neural progenitors. *Proc. Natl. Acad. Sci. USA* **106**, 16487-16492.

Seeger-Nukpezah, T. and Golemis, E. A. (2012). The extracellular matrix and ciliary signaling. *Curr. Opin. Cell Biol.* **24**, 652-661.

Shitamukai, A. and Matsuzaki, F. (2012). Control of asymmetric cell division of mammalian neural progenitors. *Dev. Growth Differ.* **54**, 277-286.

Shitamukai, A., Konno, D. and Matsuzaki, F. (2011). Oblique radial glial divisions in the developing mouse neocortex induce self-renewing progenitors outside the germinal zone that resemble primate outer subventricular zone progenitors. *J. Neurosci.* **31**, 3683-3695.

Sirakov, M., Skah, S., Nadjar, J. and Plateroti, M. (2012). Thyroid hormone's action on progenitor/stem cell biology: New challenge for a classic hormone? *Biochim. Biophys. Acta* **1830**, 3917-3927.

Takagi, J., Petre, B. M., Walz, T. and Springer, T. A. (2002). Global conformational rearrangements in integrin extracellular domains in outside-in and inside-out signaling. *Cell* **110**, 599-11.

Taverna, E., Haffner, C., Pepperkok, R. and Huttner, W. B. (2011). A new approach to manipulate the fate of single neural stem cells in tissue. *Nat. Neurosci.* **15**, 329-337.

Tzima, E., del Pozo, M. A., Shattil, S. J., Chien, S. and Schwartz, M. A. (2001). Activation of integrins in endothelial cells by fluid shear stress mediates Rho-dependent cytoskeletal alignment. *EMBO J.* **20**, 4639-4647.

Wang, X., Tsai, J. W., LaMonica, B. and Kriegstein, A. R. (2011). A new subtype of progenitor cell in the mouse embryonic neocortex. *Nat. Neurosci.* **14**, 555-561.

Yee, K. L., Weaver, V. M. and Hammer, D. A. (2008). Integrin-mediated signalling through the MAP-kinase pathway. *IET Syst. Biol.* **2**, 8-15.

Yoon, K. J., Koo, B. K., Im, S. K., Jeong, H. W., Ghim, J., Kwon, M. C., Moon, J. S., Miyata, T. and Kong, Y. Y. (2008). Mind bomb 1-expressing intermediate progenitors generate notch signaling to maintain radial glial cells. *Neuron* **58**, 519-531.

Zappaterra, M. D., Lisgo, S. N., Lindsay, S., Gygi, S. P., Walsh, C. A. and Ballif, B. A. (2007). A comparative proteomic analysis of human and rat embryonic cerebrospinal fluid. *J. Proteome Res.* **6**, 3537-3548.

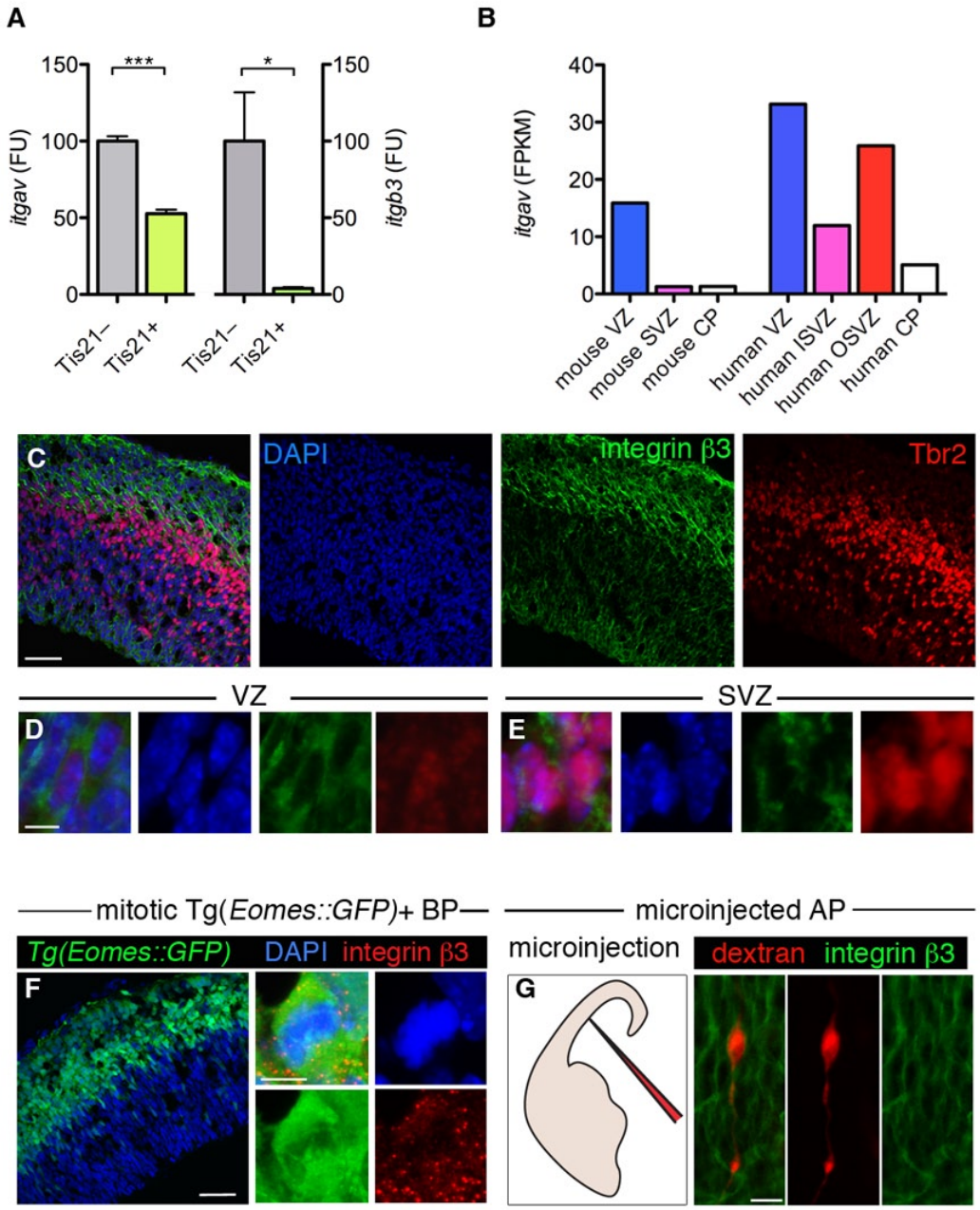

Fig. S1. Presence of integrin β_3 on APs and BPs in the E14.5 mouse neocortex. (A) Quantification of integrin αv (*itgav*, left) and integrin β3 (*itgb3*, right) mRNA in *Tis21*-GFP+ (Tis21+, green columns) compared to *Tis21*-GFP– (Tis21–, grey columns) progenitors isolated from E14.5 mouse neocortex (Arai et al., 2011). Fluorescence units (FU) for Tis21+ are expressed as percentage of Tis21–. *Itgav* FU is the mean of 3 datasets analyzed with 2 independent probes. *Itgb3* FU is the mean of 3 datasets analyzed with one probe. Error bars indicate s.d. * $P \leq 0.05$, *** $P \leq 0.001$. (B) Quantification of integrin αv (*itgav*) mRNA in E14.5 mouse VZ (blue), SVZ (purple) and CP (white) and gestational week 13-16 human VZ (blue), inner SVZ (ISVZ, purple), outer SVZ (OSVZ, red) and CP (white) (Fietz et al., 2012). Average FPKM values are shown. (C) Representative images (coronal section, 2.96-µm stacks) showing immunofluorescence for integrin β_3 (green, ab75872), Tbr2 (red) and DAPI staining (blue) of E14.5 mouse neocortex. Scale bar 50 µm. Note the strongest integrin β_3 immunoreactivity in the VZ, CP and at the basal lamina and a lower signal in the SVZ, identified by double immunofluorescence for the BP marker Tbr2, suggesting that integrin β_3 expression is higher in mouse APs than BPs and included the AP basal process endfeet contacting the basal lamina. (D,E) High magnification images (2.96-µm stacks) of immunofluorescently labeled Tbr2+ (red) basal progenitor in VZ (D) and SVZ (E) revealing co-immunostaining for integrin β_3 (green, ab75872). Scale bar 5 µm. Note that the weakly Tbr2+ newborn BPs in the VZ show integrin β_3 immunoreactivity at the plasma membrane. The same was observed for double-labeled BPs in the SVZ, albeit with a lower level of integrin β_3 immunoreactivity. (F) Overview image (3.6-µm stack) of E14.5 neocortex of Tg(*Eomes*::*GFP*) BAC transgenic mice expressing GFP under the control of the Tbr2 (Eomes) promotor (left). High magnification images (3.6-µm stack) of immunofluorescence for integrin β_3 (red, ab47584; right bottom panel) co-localizing with *Eomes::GFP* positive mitotic BP (green, left bottom panel). Blue, DAPI. Scale bar 5 µm. (G) Schematic representation of microinjection technique (Taverna et al., 2011) (left panel). Single cell visualization by microinjection

of dextran A594 (red); 50 µm coronal section of E14.5 mouse neocortex was immunostained for integrin β_3 (green, ab75872), which localizes to basolateral plasma membrane of AP. Scale bar 10 µm. Single optical section z=0.78 µm. (H-L) Correlative light microscopy and EM (Paridaen et al., 2013) of E14.5 mouse neocortex ultrathin cryosections (Dubreuil et al., 2007). (H,I) Correlative light microscopy (LM) images are shown as single channels (integrin β_3: left, DAPI: middle) and merge (integrin β_3, red; DAPI, blue). Black hexagonal bars are visible from the EM support grid. Note that the two distinct integrin β_3 antibodies on 70-nm coronal sections revealed integrin β_3 immunofluorescence throughout the cortical wall, reflecting the same localization pattern as observed by conventional immunofluorescence. (J-L) EM micrographs. Mitotic BPs (J) and interphase BPs (K, as concluded from their position in the SVZ and the chromatin arrangement as well as the abventricular location of a centriole; overview images to the left; boxed areas are shown at higher magnification to the right). Interphase APs (L) at the ventricular surface (v). Pink arrowheads indicate 10-nm gold particles for integrin β_3 (using the antibodies, Table S1), black arrowheads indicate adherens junctions. Arrows indicate the basal lamina (in LM and EM images). c: primary cilium, *: centriole, m: mitochondrium, n: nucleus. Scale bars for LM images (in merge) 10 µm, for EM overviews: 1 µm and for magnifications 100 nm. Note the integrin β_3 immunogold-labeled mitotic and interphase BPs, as well as APs residing at the ventricle, confirming the presence of integrin β_3 intracellularly and at the plasma membrane. Mitotic BPs, identified by their abventricular localization, show immunogold particles close to the membrane. Similar to the integrin β_3 immunofluorescence, the abundance of immunogold particles is higher in APs than BPs, further supporting that integrin β_3 is present in BPs, albeit at lower levels than in APs.

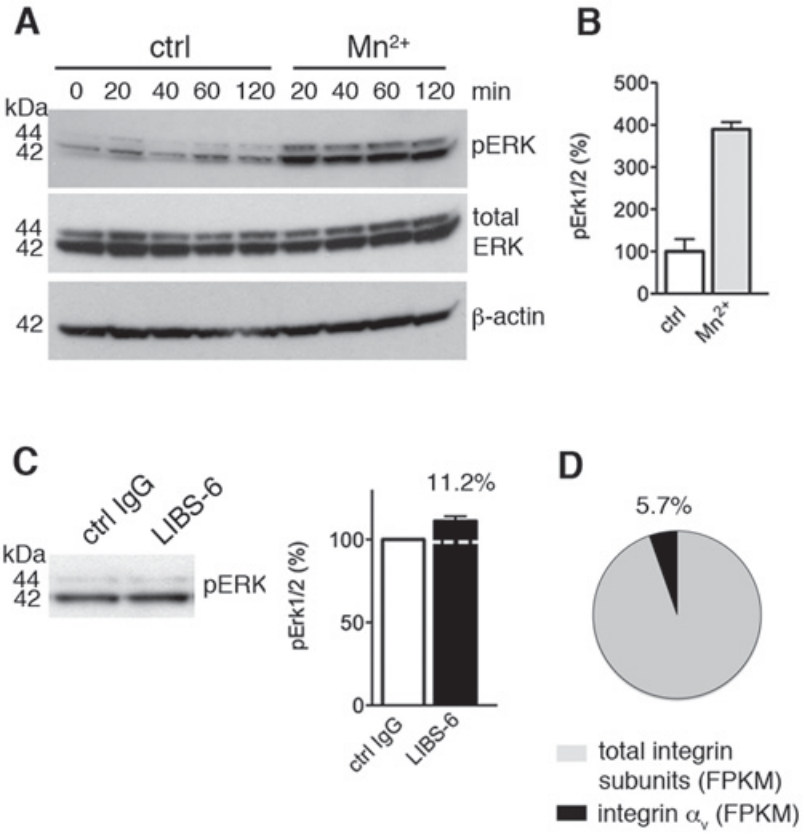

Fig. S2. Integrin activation by manganese and LIBS-6 in HERO culture. (A) E14.5 mouse HERO culture in presence or absence of 500 µM manganese (Mn^{2+}) for 0, 20, 40, 60 or 120 minutes, followed by immunoblot analysis for phosphoERK (pERK) and total ERK protein. β-Actin immunoblot serves as a protein loading control. Note that Mn^{2+} has previously been established to activate integrins by changing their conformation from an inactive, bent integrin heterodimer to an open, active conformation (Takagi et al., 2002). Integrin activation is revealed by MAP kinase signaling, a well-characterized pathway downstream of integrins (Yee et al., 2008), which has been shown to be important for progenitor cell proliferation in the cerebral cortex (Pucilowska et al., 2012). Addition of Mn^{2+} results in an increase in phosphoERK levels compared to control without altering the total level of ERK. (B) Quantification of phosphoERK immunoblot (mean of 20- and 40-minutes samples) shown in (A). Bars indicate the variation of the two values from the mean. Note the fourfold increase in the presence of Mn^{2+}, suggesting that Mn^{2+} leads to an activation of integrins present in E14.5 mouse neocortex. (C) Left: E14.5 mouse HERO culture in presence of ctrl IgG or LIBS-6 for 30 minutes followed by immunoblot for phosphoERK. Right: Quantification of the phosphoERK immunoblot shown on the left and another similar immunoblot after

60 minutes of HERO culture. Bars indicate the variation of the two values from the mean. (D) Pie chart showing the percentage of integrin α_v mRNA (black) of total integrin subunit mRNAs expressed in the E14.5 mouse cerebral cortex. Average FPKM values of the sum of VZ, SVZ and CP (Fietz et al., 2012). Note that in accordance with this relative abundance of integrin $\alpha_v\beta_3$ in the E14.5 mouse neocortex, which comprises only ≈6% of all integrins, LIBS-6 addition resulted in an 11% increase in phosphoERK compared to ctrl IgG. (C,D) Although the LIBS-6 antibody recognizes and activates not only integrin $\alpha_v\beta_3$ but also integrin $\alpha_{IIb}\beta_3$ (Frelinger et al., 1991), it can be considered to specifically target integrin $\alpha_v\beta_3$ under the present conditions because integrin α_{IIb} is not expressed in the mouse E14.5 neocortex (Fietz et al., 2012), consistent with integrin $\alpha_{IIb}\beta_3$ being characteristically expressed on platelets. In light of the specificity of the LIBS-6 antibody under the present experimental conditions, this strongly suggests that LIBS-6 can be used to activate integrin $\alpha_v\beta_3$ in HERO culture.

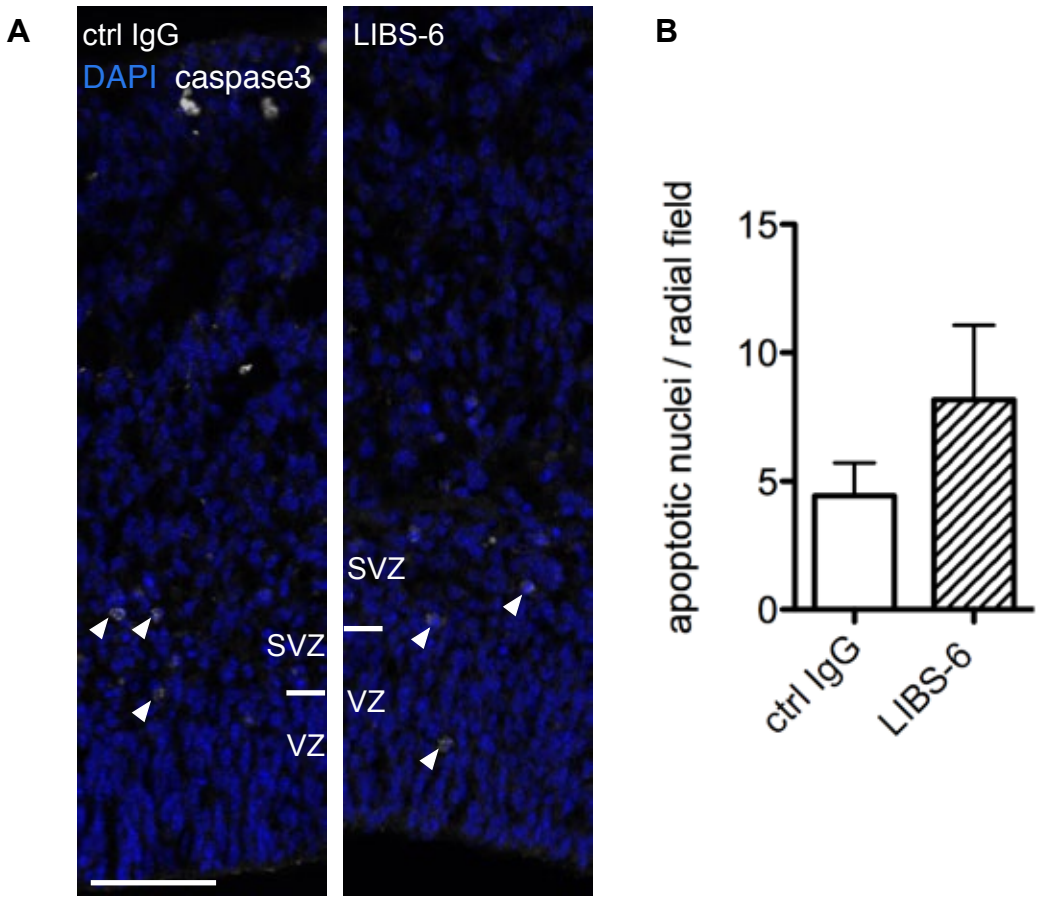

Fig. S3. Integrin $\alpha_v\beta_3$ activation does not affect cell survival. (A,B) 48-hour HERO culture of E14.5 mouse dorsal telencephalon in the presence of ctrl IgG or LIBS-6. (A) Representative images (single 1.91 µm optical section) of neocortex after culture in the presence of ctrl IgG (left) or LIBS-6 (right) showing immunofluorescence for active caspase 3 (white) and DAPI staining (blue). Boundary of VZ and SVZ is indicated. White arrowheads indicate apoptotic nuclei. Scale bar 50 µm. (B) Quantification of apoptotic nuclei in VZ plus SVZ per radial field (over 100 µm of ventricular surface length). Data are the mean of 5 hemispheres. Error bars indicate SEM.

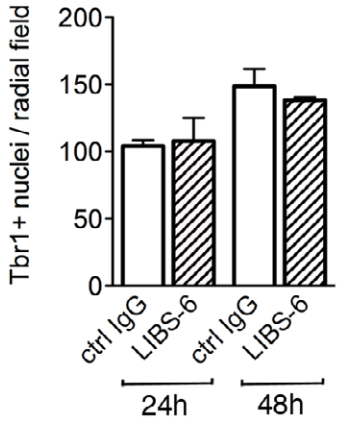

Fig. S4. Integrin $\alpha_v\beta_3$ activation does not increase neuron number per radial field. Quantification of Tbr1+ nuclei per radial field (over 100 μm of ventricular surface length) after 24 hour and 48 hour of HERO culture in the presence of ctrl IgG or LIBS-6. Data represent the mean of 4-8 radial fields from 2 hemispheres. Error bars indicate SEM.

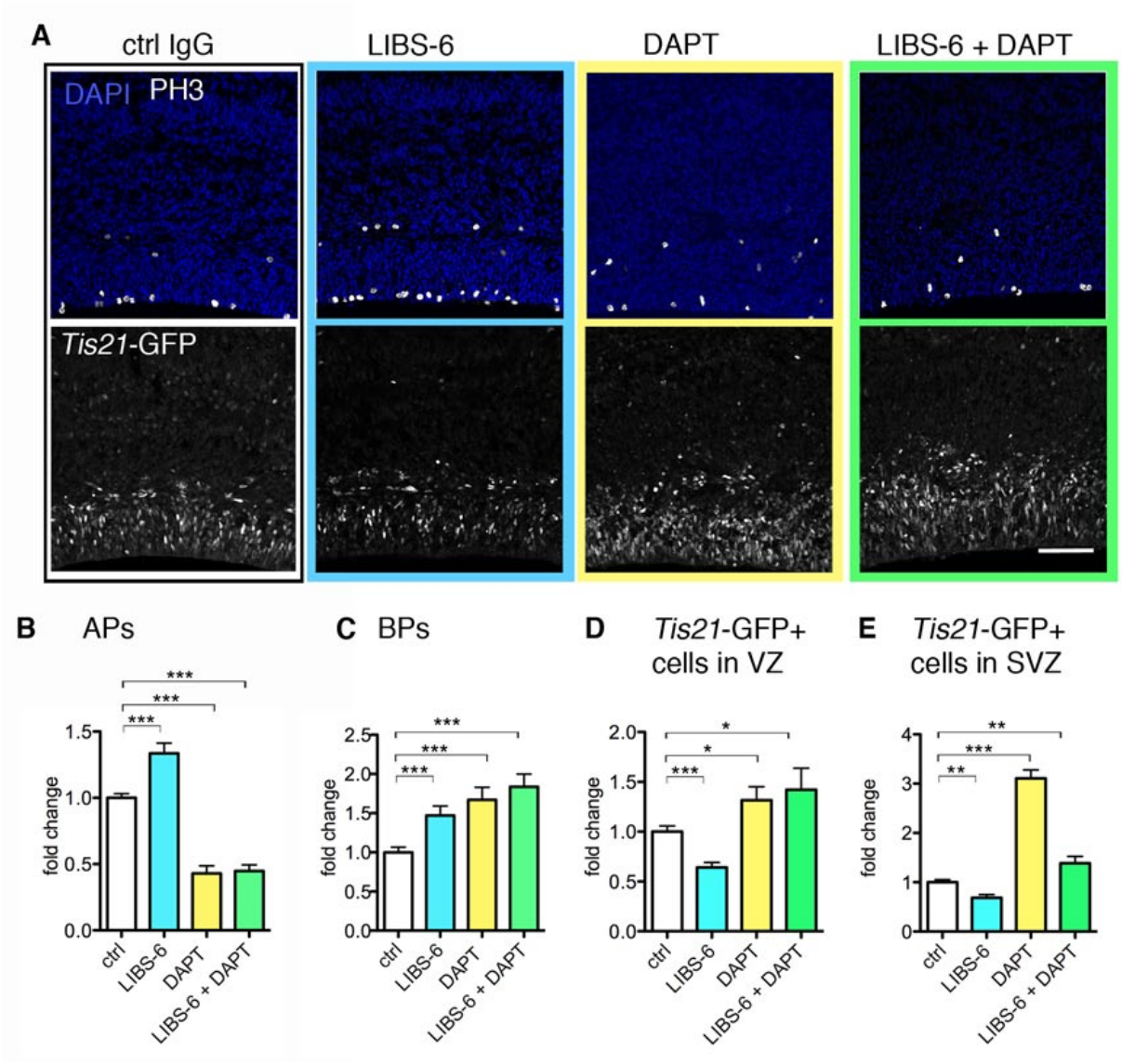

Fig. S5. Differential effects of Notch inhibition on APs Versus BPs upon integrin $\alpha_v\beta_3$ activation. To investigate whether the integrin $\alpha_v\beta_3$-stimulated proliferation of APs and BPs involves Notch signaling, we performed 48-hour HERO cultures of E14.5 mouse dorsal telencephalon from *Tis21*-GFP mice under six different conditions, i.e. in the presence of either ctrl IgG, DMSO, IgG+DMSO, LIBS-6, 10 μM DAPT, or LIBS-6+DAPT. DAPT is a γ-secretase inhibitor previously used to inhibit Notch signaling in cortical progenitors (Hansen et al., 2010). (A) Representative images (single 0.74-μm optical section) of neocortex cultured under four of the above conditions, showing immunofluorescence for PH3 (white, top panels), *Tis21*-GFP (white, bottom panels) and DAPI staining (blue). Scale bar 50 μm. Immunofluorescence for *Tis21*-GFP expression and DAPI staining in presence of LIBS-6 are the same as in Fig. 5A and are depicted again to allow comparison with the other three conditions.(B,C) Quantification (in microscopic fields of 250 μm×250 μm) of mitotic (PH3+) APs (B) and BPs (C) in ctrl (white columns), LIBS-6 (blue columns), DAPT (yellow columns), and DAPT+LIBS-6 (green columns) –treated HERO cultures. Data are the mean of 8 hemispheres and expressed as fold change relative to ctrl (average of three conditions, ctrl IgG, DMSO, and IgG+DMSO). The original data used for (C, white and blue columns, ctrl versus LIBS-6) are partly the same as those shown in Fig. 3B. (D,E) Quantification (in radial fields, over 100 μm of ventricular surface length) of *Tis21*-GFP+ cells in VZ (D) and SVZ (E) in ctrl (white columns), LIBS-6 (blue columns), DAPT (yellow columns), and DAPT+LIBS-6 (green columns) –treated HERO cultures. Data are the mean of 4 hemispheres and expressed as fold change relative to ctrl (see above). (B-E) Error bars indicate SEM. * $P \leq 0.05$, ** $P \leq 0.01$, *** $P \leq 0.001$. Note that inhibition of Notch signaling by DAPT results in a reduction of mitotic APs and an increase in mitotic BPs, suggesting that APs increasingly generate BPs, in line with previous studies (Yoon et al., 2008; Imayoshi et al., 2010). Concomitant with this effect, inhibition of Notch signaling results in an increase in *Tis21*-GFP+ progenitors in interphase in the VZ and even more so in the SVZ. In contrast to inhibition of Notch signaling, integrin $\alpha_v\beta_3$ activation by LIBS-6 results in an increase in both, mitotic AP levels and mitotic BP levels. Inhibition of Notch signaling completely blocks the integrin $\alpha_v\beta_3$–mediated increase in APs, but not that in BPs. The integrin $\alpha_v\beta_3$–mediated decrease in *Tis21*-GFP+ progenitors in interphase in the VZ is blocked by inhibition of Notch signaling. Integrin $\alpha_v\beta_3$ activation by LIBS-6 causes a substantial decrease in *Tis21*-GFP+ progenitors in interphase in the SVZ in both, the absence and presence of DAPT. In summary, Notch signaling appears to be involved in the integrin $\alpha_v\beta_3$–mediated stimulation of AP, but BP, proliferation, and hence the integrin $\alpha_v\beta_3$–mediated increase in BPs does not appear to be due to an increased production of BPs from APs or to increased AP delamination.

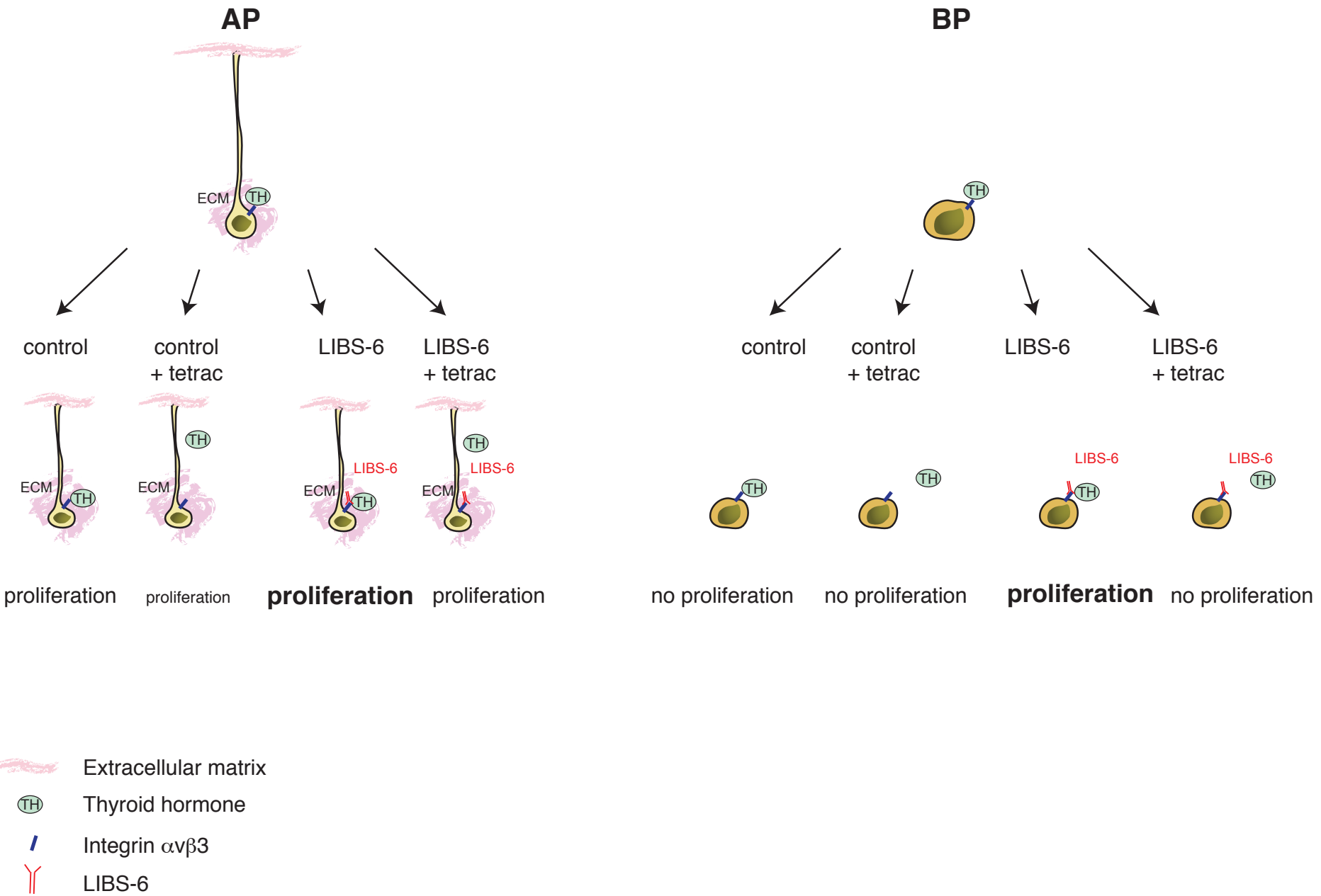

Fig. S6. Cartoon illustrating the putative effects of ECM, thyroid hormones and LIBS-6 on AP and BP proliferation via integrin $\alpha_v\beta_3$. For details, see Results and Discussion.

Table S1. Antibodies

Antibody	Method	Supplier	Dilution
Rat anti-phosphohistone H3	IF	Abcam, ab10543	1:500
Rabbit anti-Pax6	IF, FC	Covance, PRB-278P	1:200
Mouse anti-PCNA	IF, FC	Chemicon, MAB424	1:200
Rabbit anti Tbr2	IF, FC	Abcam, ab23345	1:200
Mouse anti-phosphovimentin	IF	Abcam, ab2265	1:200
Rabbit anti Ki67	IF	Abcam, ab15580	1:200
Goat anti GFP	IF	P.E.P.	1:1,500
Mouse anti-Tuj1	IF	Covance MMS-435P	1:500
Rabbit anti-Tbr1	IF, FC	Abcam, ab31940	1:200
Rabbit anti-integrin β_3	IF, EM	Abcam, ab75872	1:200
Rabbit anti-integrin β_3	IF, EM	Abcam, ab47584	1:200
Rabbit anti-active caspase 3	IF	Abcam, ab2302	1:500
Rabbit anti- human phosphoERK	WB	Cell Signaling, #4370	1:5,000
Mouse anti total ERK	WB	Cell Signaling, #4696	1:1,000
Rabbit anti-b-actin	WB	Abcam, ab8227	1:1,000
DAPI	IF	Sigma	1:1,500
Propidium iodide	FC	Abcam, ab14083	1:500
Donkey secondary antibodies conjugated to Alexa fluorophores A488, A555, A594, A647	IF, FC	Molecular Probes	1:500
Goat secondary antibodies conjugated to HRP	WB	Jackson ImmunoResearch	1:20,000

Immunofluorescence, IF; flow cytometry, FC; western blot, WB.

Table S2. Thyroid hormone serum levels after MMI treatment

	T3 (nmol/l)	T4 (nmol/l)
E16.5		
ctrl	0.66	27.06
MMI	n.d.	n.d.
ctrl	0.66	25.77
MMI	n.d.	n.d.
ctrl	0.63	29.6
MMI	n.d.	n.d.
ctrl	0.82	27.1
MMI	n.d.	n.d.
ctrl	0.59	22
MMI	n.d.	n.d.
E19.5		
ctrl	0.52	11.6
MMI	n.d.	n.d.
ctrl	0.51	21.9
MMI	n.d.	n.d.
ctrl	0.54	29
MMI	n.d.	n.d.
mouse (14d)		
ctrl	0.91	81
MMI	0.99	43

The serum levels of thyroid hormones, that is, thyroxine (T4) and triiodothyronine (T3), were determined by radioimmunoassay as previously described (Friedrichsen et al., 2003) for control (ctrl) and MMI-treated E16.5 (5 pairs) and E19.5 (3 pairs) pregnant rats and for 14 day (d) control (ctrl) and MMI-treated adult mice. Blood samples of MMI-treated and control pregnant rats, and of MMI-treated and control mice, were (after clotting) centrifuged at 2,000x*g* for 5 minutes at RT to obtain serum. Note that MMI treatment of mice did not result in sufficient reduction of thyroid hormone serum levels, possibly due to higher metabolic rate in mice compared to rats. n.d. not detectable.